POLITECNICO DI TORINO
Repository ISTITUZIONALE

Spectrum features of the eigenvalue formulations in neutron transport

Original
Spectrum features of the eigenvalue formulations in neutron transport / Abrate, N., Dulla, S., Ravetto, P., Saracco, P.. - In: ANNALS OF NUCLEAR ENERGY. - ISSN 0306-4549. - ELETTRONICO. - 201:(2024). [10.1016/j.anucene.2024.110421]

Availability:
This version is available at: 11583/2986569 since: 2024-03-05T11:26:56Z

Publisher:
Elsevier

Published
DOI:10.1016/j.anucene.2024.110421

Terms of use:

This article is made available under terms and conditions as specified in the corresponding bibliographic description in the repository

Publisher copyright

(Article begins on next page)

30 October 2026

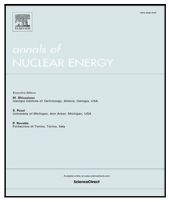
Annals of Nuclear Energy 201 (2024) 110421



Contents lists available at ScienceDirect

Annals of Nuclear Energy

journal homepage: www.elsevier.com/locate/anucene



Spectrum features of the eigenvalue formulations in neutron transport

Nicolò Abrate [a,b,*], Sandra Dulla [a,b], Piero Ravetto [a,b], Paolo Saracco [b]

[a] Politecnico di Torino, Dipartimento Energia, Corso Duca degli Abruzzi, 24 - 10129 Torino, Italy
[b] Istituto Nazionale di Fisica Nucleare (I.N.F.N.), Sezione di Genova, Via Dodecaneso, 33 - 16146 Genova, Italy

ARTICLE INFO

Dataset link: 10.5281/zenodo.10608509

Keywords:
Energy spectrum
Eigenvalue spectrum
Criticality eigenvalue
Collision eigenvalue
Density eigenvalue
Time eigenvalue

ABSTRACT

The steady state neutron transport equation can be studied resorting to different eigenvalue formulations, useful to investigate the criticality state of a nuclear system. In this respect, the knowledge of the eigenvalue spectra featuring the main eigenproblems is fundamental, from a practical standpoint, to guide the eigenvalue solvers searching for the dominant eigenpairs. The study of the eigenvalue spectrum shape on the complex plane is also relevant to better understand the physico-mathematical aspects of the neutron transport numerical approximations. This paper investigates the features of the eigenvalue spectra with respect to various parameters like modelling approximations, departure from criticality and spatial heterogeneity in a one-dimensional slab geometry framework. The sensitivity of the energy spectrum characterising the fundamental eigenfunction is then evaluated with respect to the model adopted and to perturbations in the input parameters.

1. Introduction

Non-trivial mathematical solutions of the source-free, steady state, neutron transport equation for a multiplying medium can only be found by casting the equation into the form of an eigenvalue problem,

$$\hat{A}\varphi_{\lambda} = \lambda \hat{B}\varphi_{\lambda}, \tag{1}$$

where $\hat{A}$ and $\hat{B}$ are linear operators representing some physical aspects of the transport process and the generic eigenvalue is here denoted by λ. The eigenvalue may belong to either a finite or infinite set, possibly including also a continuous part, depending on the structure of operators $\hat{A}$ and $\hat{B}$. This is a fundamental problem of nuclear reactor physics, which is usually solved with the introduction of an eigenvalue acting on the fission operator, the so-called multiplication eigenvalue k (Bell and Glasstone, 1970).

Many other possible eigenvalue formulations exist, each featured by different properties and stressing different physical aspects (Davison, 1957). The balance in Eq. (1) can be physically interpreted saying that the particle balance is satisfied when the action of $\hat{A}$ on the flux distribution $\varphi_{\lambda,i}$ is equal to the action of $\hat{B}$ scaled with a tuning parameter λ_i. The eigenvalue λ_i associated with an eigenfunction featured by a uniform sign on the domain is defined as the fundamental eigenvalue, and is usually identified with $i = 0$. In this respect, the eigenvalue turns out to be a parameter scaling some physical properties featuring the system and "encoded" in the linear operator $\hat{B}$ (e.g., the number of neutrons emitted by fission ν, the geometrical dimensions, ...). Each eigenvalue formulation leads to different eigenfunctions $\varphi_{\lambda,i}$, unless the system is critical. In this specific case, no scaling is needed to satisfy the particle balance, and all the eigenvalue formulations yield the same eigenfunction, describing the critical distribution of neutrons in the phase space.

Although it is not always possible attributing a physical interpretation to each eigenfunction in off-critical situations, the eigenfunctions are often employed in several applications for reactor design and analysis, such as perturbation theory, the calculation of kinetic parameters and the generation of multi-group constants. Due to their vast practical use, the different eigenvalue problems have been investigated since the very beginning of nuclear reactor physics. After the multiplication eigenvalue k, the collision eigenvalue γ was introduced by Davison (1957). Almost one year later, Henry (1958) introduced the concept of time eigenvalue, which is tightly related to the application of the Laplace transform to the neutron transport equation. About twenty years later, the density eigenvalue δ was formulated (Ronen et al., 1976) and recently generalised for core-design applications (Abrate et al., 2023). The literature on the multiplication and time eigenvalues is very rich, covering both theoretical aspects (see Sahni and Sjöstrand (1990), Sanchez and Tomatis (2019) and McClarren (2019) for transport theory and Saracco et al. (2012), Sanchez et al. (2017) and Dulla et al. (2018) for diffusion theory) and practical applications (see, for instance, Dugan et al. (2016, 2018)), while there are only a few works focusing also on the collision and density eigenvalues. In Velarde et al.

* Corresponding author at: Politecnico di Torino, Dipartimento Energia, Corso Duca degli Abruzzi, 24 - 10129 Torino, Italy.
E-mail addresses: nicolo.abrate@polito.it (N. Abrate), sandra.dulla@polito.it (S. Dulla), piero.ravetto@polito.it (P. Ravetto), paolo.saracco@ge.infn.it (P. Saracco).

https://doi.org/10.1016/j.anucene.2024.110421
Received 3 October 2023; Received in revised form 2 February 2024; Accepted 10 February 2024
Available online 1 March 2024
0306-4549/© 2024 The Author(s). Published by Elsevier Ltd. This is an open access article under the CC BY license (http://creativecommons.org/licenses/by/4.0/).

(1978) and Cacuci et al. (1982) the eigenvalue-dependent neutron energy spectra are compared for fast and thermal systems, with a focus on the behaviour of the spectral indexes, while in Carreño et al. (2017) and Carreño et al. (2019) the higher-order eigenfunctions computed with the time, multiplication and collision formulations are applied in the framework of a modal expansion method to solve the time-dependent diffusion equation for full-core analysis. At last, in Kiedrowski (2012, 2014) the adoption of the Monte Carlo method to compute the time, multiplication and collision eigenfunctions is presented, focusing on the adoption of these spectra to generate the kinetic parameters for point kinetics.

The works mentioned so far are mainly devoted to applications involving these alternative eigenfunctions, but do not investigate more theoretical aspects that could have an important impact on their calculation and final usage, such as the behaviour of the eigenvalue spectrum. The main objective of this work is to investigate some fundamental properties of the eigenvalue problems mentioned, trying to get some insights that could be useful for the application of these eigenfunctions in reactor analysis. The first part of the paper introduces the most popular eigenvalue problems arising in neutron transport, focusing on their eigenvalue spectrum, whose distribution in the complex plane is fundamental to properly tune the numerical solvers employed to determine the dominant harmonics. The second part of the work focuses on the sensitivity of the energy spectrum featuring the various formulations with respect to input parameters (e.g., cross sections) and to the neutron transport model adopted to estimate it (e.g., the angular expansion order). Since approaching this study analytically would be challenging, the investigations are carried out numerically, relying on the P_N and S_N approximations of the one-dimensional, multi-group neutron transport equation, which is discretised spatially with the finite difference scheme.

2. The neutron transport model in plane geometry

The neutron transport model in the absence of an external source is described by the following system of equations, expressed compactly with a set of integro-differential linear operators,

$$\begin{cases} \frac{1}{v(E)}\frac{\partial \phi}{\partial t} + \hat{L}\phi + (\hat{C} + \hat{F}_T + \hat{S}_T)\phi = \hat{S}\phi + \hat{F}_p\phi + \sum_{r=1}^{R} \lambda_r \epsilon_r \\ \frac{\partial \epsilon_r}{\partial t} = \hat{F}_{d,r}\phi - \lambda_r \epsilon_r \quad r = 1, \dots, R, \end{cases} \tag{2}$$

subject to appropriate initial and boundary conditions. The various operators have the following definitions for the case of a one-dimensional cartesian system:

- the streaming operator,

$$\hat{L} = \mu \frac{\partial}{\partial x} *; \tag{3}$$

- the removal by collision operator, which can be seen as the sum of capture, fission and scattering,

$$\begin{aligned} \hat{R} &= \Sigma_t(x,E) *= \hat{C} + \hat{F}_T + \hat{S}_T \\ &= \Sigma_c(x,E) * + \Sigma_f(x,E) * + \Sigma_s(x,E) *; \end{aligned} \tag{4}$$

- the scattering operator, assuming that the number of neutrons emitted by scattering ν_s ranges between 1 and 4, accounting for the (n,xn) reactions,

$$\hat{S} = \int_0^\infty dE' \int_{-1}^{1} d\mu' \, \nu_s(E') \Sigma_s(x,E') f_s(x, E' \to E, \mu') *; \tag{5}$$

- the prompt fission operator,

$$\hat{F}_p = (1-\beta)\frac{\chi_p(x,E)}{2} \int_0^\infty dE' \int_{-1}^{1} d\mu' \, \nu \Sigma_f(x,E') *; \tag{6}$$

- the delayed fission operator for the rth delayed precursor family,

$$\hat{F}_{d,r} = \beta_r \frac{\chi_{d,r}(x,E)}{2} \int_0^\infty dE' \int_{-1}^{1} d\mu' \, \nu \Sigma_f(x,E') * . \tag{7}$$

At last, the delayed emissivity for the rth delayed precursor family is defined as:

$$\epsilon_r(x,E,t) = \frac{\chi_{d,r}(x,E)}{2} C_r(x,t). \tag{8}$$

The other symbols have their usual meaning, as it can be found in most reactor physics books (Bell and Glasstone, 1970; Duderstadt and Hamilton, 1976).

In the following sections, these operators are assumed to be discretised in energy with the multi-group approach, approximated in angle with the P_N or S_N methods and discretised in space with the finite difference scheme (Lewis and Miller, 1984). The numerical calculations are carried out with an *in-house* Python package, called TEST (Transport Equation Solver in Turin). More details on the numerical implementation of this code and its capabilities can be found in Abrate et al. (2019, 2021b, 2023), and the code package is publicly available on GitHub.

3. Spectrum analysis of the eigenvalue formulations in neutron transport

In this section, the various eigenvalue problems are presented. The behaviour of each spectrum is studied as a function of different modelling parameters, like the number of spatial meshes N_x, the angular expansion order N and number of groups G. Each approximation to Eq. (2) introduces a number of degrees of freedom (DoF) equal to the rank of the discretised transport operator and, thus, of eigenvalues. The number of DoF featuring the P_N model can be computed as

$$DoF = \begin{cases} G\frac{N+1}{2}(2N_x - 1), \ N = 1, 3, 5 \dots \\ G\frac{N}{2}(2N_x - 1), \ N = 2, 4, 6 \dots, \end{cases} \tag{9}$$

while the number of DoF of the S_N approach is simply given as $DoF = GNN_x$. The eigenvalue spectra are also studied as a function of some input parameters, like the spatial heterogeneity and off-criticality levels. For some selected eigenvalues, a comparison between fast and thermal systems is also carried out, focusing on configurations representative of Light Water Reactor (LWR), Molten Salt Fast Reactor (MSFR) and Lead Fast Reactor (LFR) energy spectra.

Tables 1 and 2 report the group boundaries of the structures used in the following calculations. The structures in Table 1 are nested, i.e. each grid contains the preceding one, thus ensuring a consistent comparison among different energy group grids, while the 8-group grid in Table 2 is conceived to compare different reactor energy spectra. It should be remarked here that, in order to carry out consistent comparisons among the eigenvalue formulations in the following sections, the same 50 cm thick, 1D slab reactor (and models) are used to study the effect of the various parameters. In order to ease the reader, the various eigenvalue spectra of the same system are represented with the same symbols and colours throughout the following sections.

3.1. The multiplication eigenvalue

Fermi first described the criticality concept by introducing an eigenvalue called *reproduction factor* k (Fermi, 1942) with the aim of controlling the recently discovered fission reaction (Hanh and Strassmann, 1939),

$$\hat{L}\vec{\varphi}_{k,n} + \hat{R}\vec{\varphi}_{k,n} - \hat{S}\vec{\varphi}_{k,n} = \frac{1}{k_n}\hat{F}\vec{\varphi}_{k,n}. \tag{10}$$

When the system is *sub-critical*, the eigenvalue scales ν up ($k_0 < 1$), while, when the system is *super-critical*, ν is scaled down ($k_0 > 1$). Since neutrons emitted by fissions are fast, this artificial scaling may alter

Table 1
Energy group structures employed in the following sections.

Group boundary [MeV]	8.21×10^{-1}	5.53×10^{-3}	4.00×10^{-6}	6.25×10^{-7}	1.40×10^{-7}	5.80×10^{-8}
CASMO-2				x		
CASMO-4	x	x		x		
CASMO-7	x	x	x	x	x	x

Table 2
8-group structure adopted for generating the cross sections of the LWR, LFR and MSFR cases. The energies are expressed in MeV.

8	$2 \cdot 10^{1}$	$1 \cdot 10^{0}$	$1 \cdot 10^{1}$	$1 \cdot 10^{-1}$	$1 \cdot 10^{-2}$	$1 \cdot 10^{-3}$	$1 \cdot 10^{-4}$	$1 \cdot 10^{-5}$	$6.25 \cdot 10^{-7}$	$1 \cdot 10^{-11}$

the energy spectrum of the system with respect to the critical case: in the sub-critical case there are more fissions, qualitatively resulting in a harder neutron spectrum, while in the super-critical one the spectrum may be softer. In practical cases like those discussed in Section 4, the energy spectrum hardening/softening effect with respect to the critical configuration depends also on the reactor design and on the cause of the off-criticality condition. Hence, it may not be trivial to draw *a priori* conclusions on the overall energy spectrum. The integration of Eq. (10) over the phase space allows to understand the physical meaning of the reproduction factor, or *effective multiplication factor*,

$$k_n = \frac{\langle \hat{F}\vec{\varphi}_{k,n} \rangle}{\langle (\hat{L} + \hat{R} - \hat{S})\vec{\varphi}_{k,n} \rangle}, \tag{11}$$

as the ratio between the number of neutrons produced by fission and the number of neutron losses. The reason that probably contributed the most to make the k-eigenvalue the main way of addressing criticality lies in the fact that it always yields a solution, if the system is fissile. This can be justified physically: it is always possible to achieve criticality by adjusting the multiplying properties of the fissile material. This feature is also extremely convenient from a numerical point of view, as most algorithms for the solution of eigenvalue problems, e.g., the power method (Bell and Glasstone, 1970), are tailored to compute the eigenvalues at the extremities of the spectrum. In fact, among the various eigenvalue problems analysed in this work, the k-spectrum is certainly the simplest one.

Fig. 1 shows that the shape of the k-spectrum on the complex plane is basically independent of the different numerical approximations. It should be noted that, for the sake of clarity, the spectra in the figures are shifted along the vertical axis to distinguish the solution sets. In all these cases, the eigenvalues are real and positive numbers, accumulating on the left of the fundamental eigenvalue, indicated throughout the paper with a star symbol. The first 5–6 dominant eigenvalues are roughly equal for the various models, showing a certain separation between each other, while the other ones try to reproduce the *continuum* of eigenvalues featuring the spectrum of the transport operator (Case, 1960). According to the number and type of DoFs, the higher eigenvalues tends to shift either towards the left, for increasing N_x and G, or to the right, for increasing N. Fig. 1(d) compares the P_1 and the S_2 models, which are formally equivalent only when no space discretisation occurs. The figure clearly shows that the discrepancy between the two sets of eigenvalues increases for the higher-order eigenvalues, associated with higher spatial frequencies and thus a more relevant effect of spatial discretisation. All the calculations carried out in this paper consider Mark vacuum boundary conditions.

Figs. 1(e) and 1(f) represent the effects of the off-criticality and spatial heterogeneity levels for equal DoFs. As expected, the spectrum is shifted towards the left/right and is inflated/shrunk when the system is sub-critical/super-critical, respectively. The effect of the material arrangement is investigated considering a bare reactor, a reflected reactor (composed by 30 cm thick fuel surrounded at both sides by water) and a fuel lattice (realised alternating 10 cm thick layers of water and fuel) with the same total thickness, equal to 50 cm. The reflected reactor and the lattice are depicted in Fig. 2. The spatial heterogeneity shrinks the spectrum compared to the bare case, but the specific arrangement alters the eigenvalue separation. In the reflected case the distance between the dominant eigenvalues is larger than the homogeneous case, while in the lattice case the eigenvalues tend to form couples that are progressively closer.

The numerical studies reported confirm the interesting properties of the spectrum of the k formulation. Nevertheless, this eigenproblem has two limitations that are too often ignored. The first is that, in core-design applications, k offers only qualitative information on the criticality state, since it is not possible to act directly on the multiplying properties of the system. In this respect, the recently introduced ζ eigenvalue (Abrate et al., 2023) is much more flexible. The other limitation is the fact that the k-eigenfunction can poorly describe the flux distribution for a system that is actually time-dependent, as brilliantly explained in Cullen et al. (2003).

3.2. The collision eigenvalue

Since also scattering leads to neutron emissions, Davison (1957) proposed to introduce an eigenvalue acting on all collisions producing neutrons,

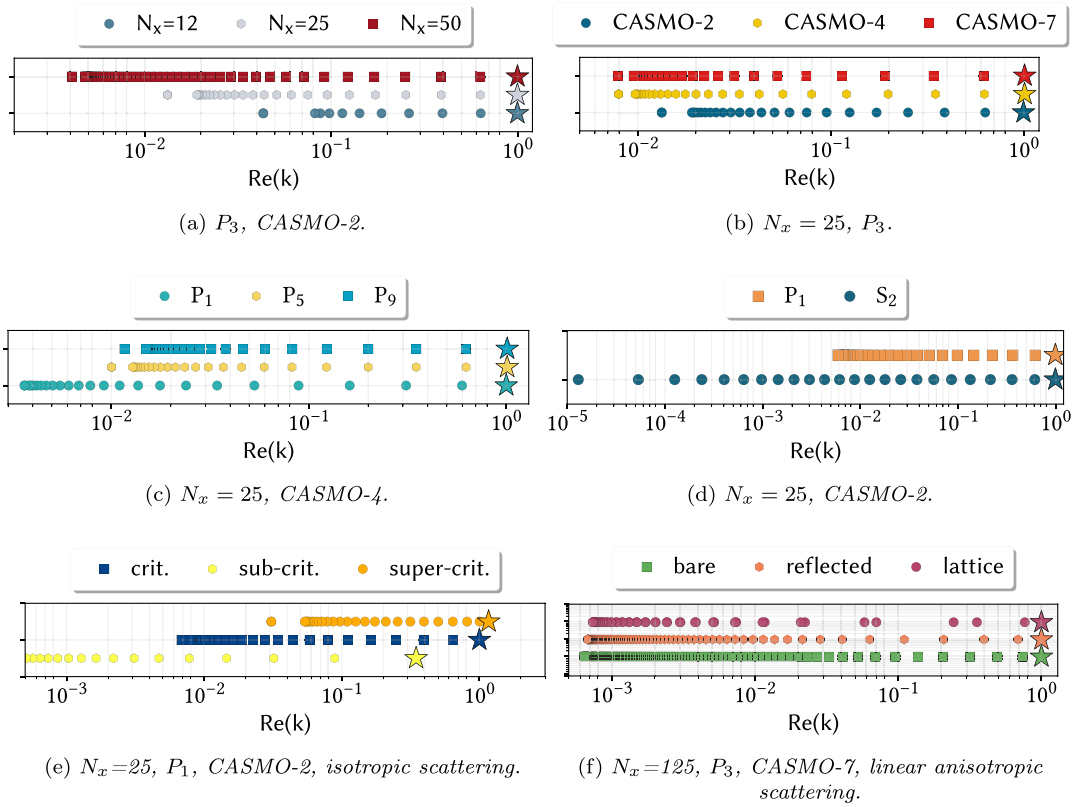
$$\hat{L}\vec{\varphi}_{\gamma,n} + \hat{R}\vec{\varphi}_{\gamma,n} = \frac{1}{\gamma}\left(\hat{S} + \hat{F}\right)\vec{\varphi}_{\gamma,n}. \tag{12}$$

Due to its collocation, γ is somehow similar to k, starting from its physical meaning, which is closely related to the number of secondaries per collision:

$$\gamma_n = \frac{\langle (\hat{F} + \hat{S})\vec{\varphi}_{\gamma,n} \rangle}{\langle (\hat{L} + \hat{R})\vec{\varphi}_{\gamma,n} \rangle}. \tag{13}$$

As for k, the system is critical when $\gamma_0 = 1$, i.e. the number of neutrons emitted is equal to the number of neutrons leaked or absorbed, while it is larger/lower than the unity when the system is super-critical/sub-critical. Since it also acts on $\hat{F}$, the γ-spectrum inherits the property of existence of a real, positive eigenvalue from k, provided that the system is multiplying. In case this condition is not met, the criticality may still be possible scaling the ν_s, i.e. the number of particles emitted from the (n, xn) multiplication reactions.

The action on $\hat{S}$ enriches the physical features of the spectrum, as visible from Fig. 3, which shows the effect of the energy and angular models for isotropic and anisotropic scatterings. Contrarily to k, the scattering anisotropy and the adoption of finer energy grids introduce some complex eigenvalues, related to angular and energy transfer effects, which do not appear when emissions are isotropic, as for fission. It should be noticed that the spectrum computed with the CASMO-2 grid is purely real only when the scattering is isotropic. The order of the scattering anisotropy strongly affects the spectrum: when a quadratic scattering is assumed, the P_5 and the P_9 spectra show additional clusters of complex eigenvalues around $\mathrm{Re}(\gamma) \in [0.2, 0.4]$ with respect to the spectrum computed with the P_1 model, which obviously is not able to take into account the second anisotropy scattering order. When the DoF are reduced, e.g. using 4 groups instead of 7 or moving from P_9 to P_1, the complex branches of coarser models try to do their best to reproduce the pattern of the finer models. For the sake of conciseness, the effect of N_x on the spectrum is not reported, being very similar to what occurs for k: the addition of spatial DoF does not alter the features of the spectrum.

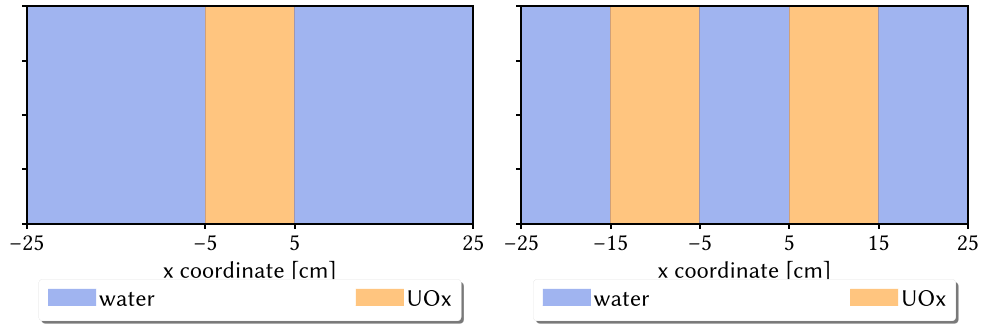


(a) P_3, *CASMO-2.* (b) $N_x = 25$, P_3.

(c) $N_x = 25$, *CASMO-4.* (d) $N_x = 25$, *CASMO-2.*

(e) N_x=*25*, P_1, *CASMO-2, isotropic scattering.* (f) N_x=*125*, P_3, *CASMO-7, linear anisotropic scattering.*

Fig. 1. k-spectrum for a homogeneous, isotropic, fissile slab.



(a) (b)

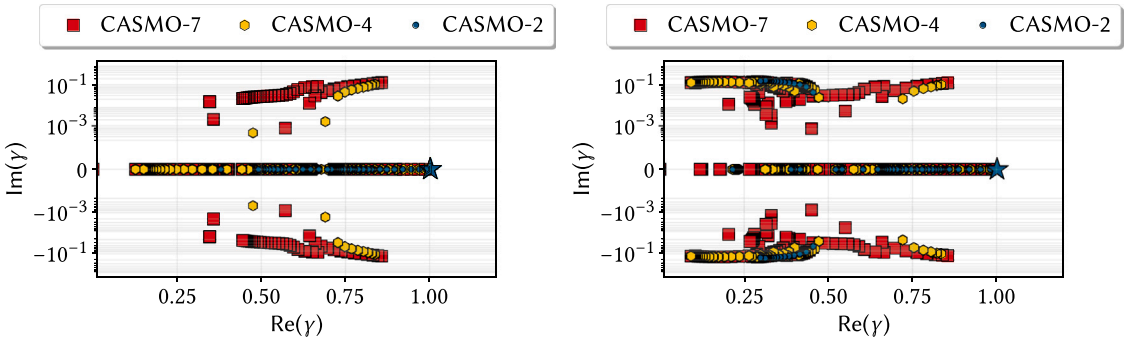
Fig. 2. Sketch of the systems adopted to study the effect of spatial heterogeneities on the eigenvalue spectrum.

Fig. 4 provides a comparison between the spectra of the P_1 and the S_2 models, which are very similar except for the high-frequency eigenvalues, and an example of the behaviour of the spectra in the presence of spatial heterogeneity. Despite some slight differences in the complex branches, it is not possible to notice specific effects induced by the heterogeneity, as for k. In this respect, it is useful to notice that k acts only on the fissile regions, while γ acts on each region because of the scatterings.

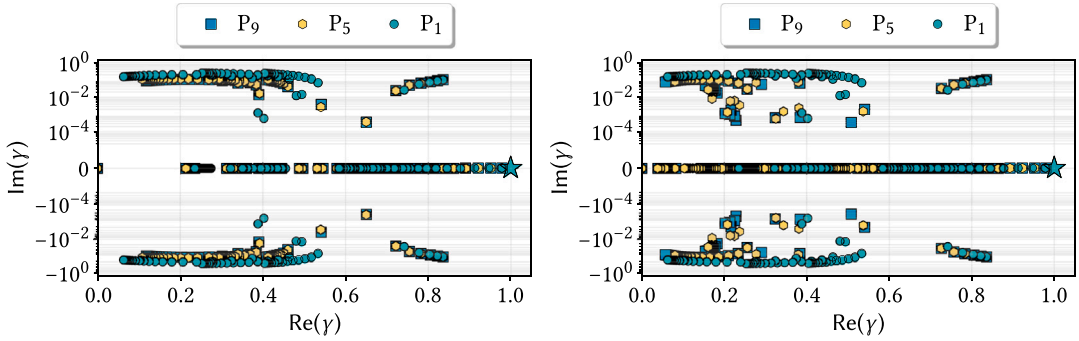
Regarding the influence of the criticality level, reported in Fig. 5(a), the γ spectrum behaves similarly to the k case, i.e. the eigenvalues tend to be more dispersed when the system is sub-critical, despite γ_0 is less sensitive than k_0 to this effect. Fig. 5(b) compares the γ-spectrum for three critical, homogeneous slabs featured by different energy spectra $\varphi(E)$, representative of a LWR, a MSFR and a LFR. The complex branches, which are related to higher-order angular and energy effects, are very sensitive to the type of reactor considered. The LWR case is featured by the largest number of complex branches, followed by the MSFR and by the LFR cases. Due to the action of γ on $\hat{S}$, this ranking suggests that the number of complex branches is proportional to the moderating capabilities of the various reactors.

3.3. The time eigenvalue

The time eigenvalue ω (indicated also with the letter α if the fission delayed neutron emissions are not considered) is the most popular one after the multiplication eigenvalue k. Firstly introduced by Henry (1964), this formulation has been extensively investigated from both theoretical (Dahl et al., 1983; Sahni and Sjöstrand, 1990; Sahni et al., 1995; Saracco et al., 2012; Dulla et al., 2018) and practical (Cacuci et al., 1982; Singh et al., 2011; Dugan et al., 2016; McClarren, 2019; Zoia et al., 2014; Vitali, 2020) aspects, due to its strong relationship with the time evolution of an off-critical system. With respect to the other formulations presented in this work, the time eigenproblem is the only natural spectral formulation of the transport equation, being associated with its Laplace transform. This operation amounts to assume

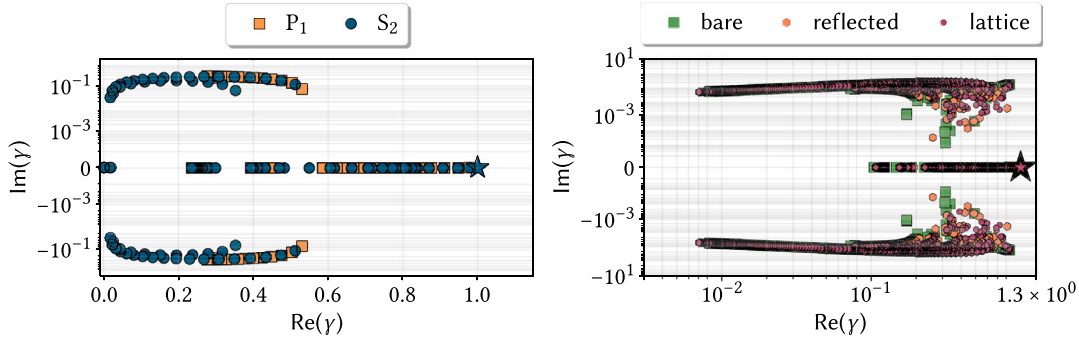


(a) P_3, *isotropic scattering.* (b) P_3, *linear anisotropic scattering.*



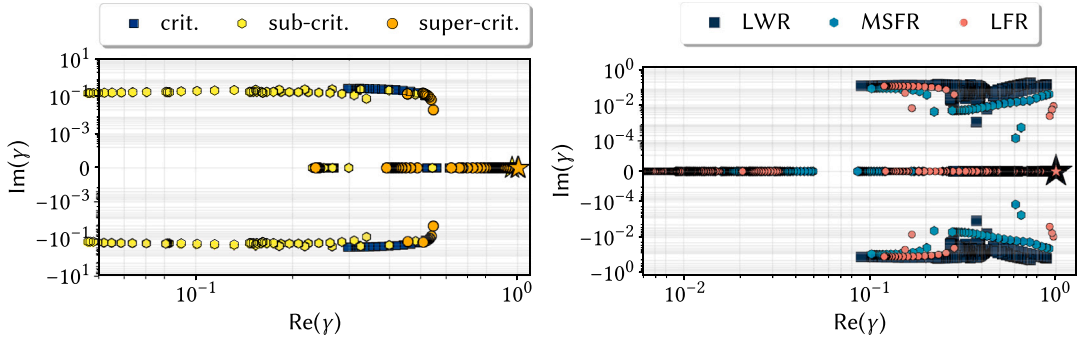
(c) *CASMO-4, linear scattering anisotropy* (d) *CASMO-4, quadratic scattering anisotropy*

Fig. 3. γ-spectrum for a homogeneous, fissile slab ($N_x = 25$).



(a) N_x=25, *CASMO-2.* (b) N_x=125, P_3, *CASMO-7.*

Fig. 4. γ-spectrum of a homogeneous, fissile slab featured by linearly anisotropic scattering (left) and of a slab featured by different levels of heterogeneity, considering linearly anisotropic scattering (right).



(a) N_x=25, P_1, *CASMO-2.* (b) N_x=25, P_3, G=8.

Fig. 5. γ-spectrum for homogeneous, fissile slabs with linearly anisotropic scattering.

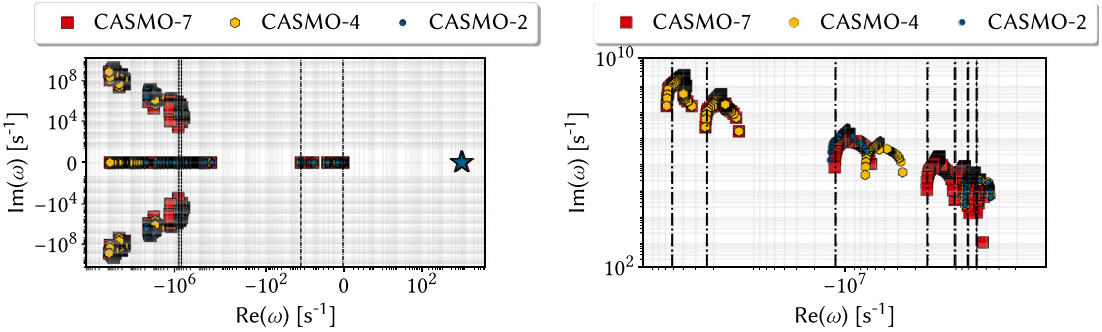


Fig. 6. Full ω-spectrum (left) and its enlargement (right) for a homogeneous, fissile slab, whose cross sections are collapsed according to the energy structures indicated ($N_x = 25$, P_3). The dashed black lines indicate the mean collision frequency for the CASMO-7 grid. The scattering is assumed linearly anisotropic.

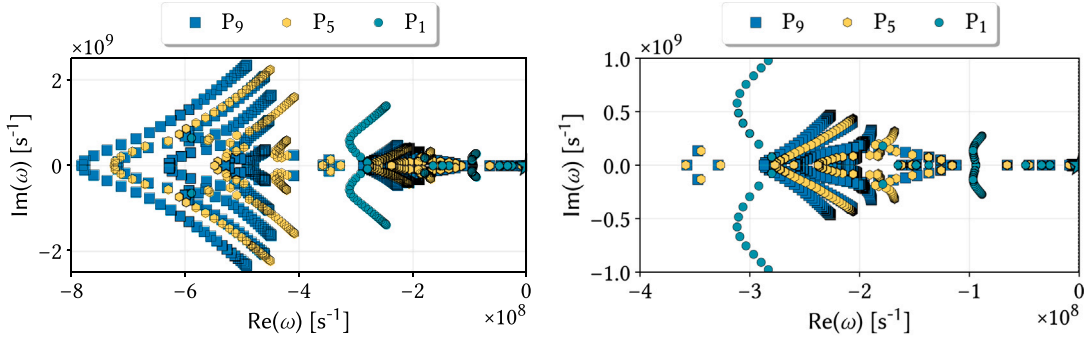


Fig. 7. Time spectrum with delayed neutrons of a homogeneous, fissile slab with isotropic scattering (N_x = 25, CASMO-4). The top graph shows the full spectrum, while the bottom ones show two enlargements.

that both the neutron flux and the precursor concentrations follow an exponential decay,

$$\phi(x, E, \vec{\mu}, t) = \varphi_{\omega,n}(x, E, \vec{\mu}) e^{\omega_n t}. \tag{14}$$

The last equation, which allows to cast Eq. (2) as an eigenproblem of R + 1 equations, allows to identify the ω_n eigenvalues as time frequencies and the eigenfunctions as the modes featuring the system free evolution. In particular, ω_0 is the inverse of the reactor stable period, which is a fundamental kinetic parameter in presence of delayed emissions. The combination of the neutron transport equation and the equations for the precursors concentrations yields a non-linear eigenproblem equivalent to Eq. (2),

$$\hat{L}\vec{\varphi}_{\omega,n} + \left(\hat{R} + \omega_n \hat{T}\right)\vec{\varphi}_{\omega,n} = \hat{S}\vec{\varphi}_{\omega,n} + \hat{F}_p\vec{\varphi}_{\omega,n} + \sum_{i=1}^{R} \frac{\lambda_i}{\omega_n + \lambda_i} \hat{F}_i \vec{\varphi}_{\omega,n}. \tag{15}$$

Analytical and numerical studies have shown that the ω-spectrum may be featured by both a discrete and a continuous part. The presence of a continuous spectrum depends on the transport model adopted and on the approximation employed, as well as on the particular system geometrical configuration. For example, a continuous spectrum can appear also in diffusion theory, when infinite media are considered (Chentre et al., 2018).

Another well-known aspect is the presence of clusters of discrete eigenvalues, known as *delayed frequencies*, associated with the delayed neutron emissions. As proved by Henry (1958), the delayed eigenvalues accumulate at the right of each $-\lambda_i$, $\forall i = 1, \ldots, R$. The eigenpair clustering, tightly related to the nature of the inhour equation (Sanchez and Tomatis, 2019), justifies the presence of eigenstates featured by very similar fluxes but different precursors spatial concentrations. Each eigenstate $(\vec{\varphi}_{\omega,n}, \vec{\varepsilon}_{\omega,n,i})$ in a cluster is important for the physical description of the system dynamics, despite only the eigenstate associated with $\omega + \lambda_1 > 0$ has a uniform sign (Ravetto, 1974). When $\omega + \lambda_i < 0$, $\vec{\varphi}_{\omega,n} > 0$ but $\vec{\varepsilon}_{\omega,n,i} < 0$. Clustering is an issue for any numerical algorithm aiming at retrieving only the dominant eigenvalues, especially for sub-critical and close-to-critical systems when the dominant eigenpairs are close to the cluster.

Due to its collocation in Eq. (15), the term $\omega/v(E)$ is often referred to as *time absorption*, although *time capture* is more appropriate, as the fission cross section is not modified. The time capture "cross section" $\Sigma_{\omega,c}(E)$ can be physically interpreted as a virtual reaction featured by a $1/v(E)$ spectrum (Weinberg and Wigner, 1958). For critical systems, the fundamental eigenvalue ω_0 vanishes, while for off-critical cases, there are two possibilities: for super-critical systems, $\Sigma_{\omega,c}(E)$ hardens the neutron spectrum, being positive and larger at lower energies; for sub-critical systems, $\Sigma_{\omega,c}(E)$ softens the neutron spectrum, being negative and lower at lower energies. The virtual capture can cause some numerical issues: when $\Sigma_t + \omega/v < 0$ (or close to zero), the transport solver (inner iterations) may experience some numerical instabilities, and the search for the fundamental eigenvalue may be difficult in the case the state of the system is not known (as it generally occurs). Concerning the impact of the modelling approximations on the spectrum, increasing N_x does not alter its shape, as already observed for the k and γ. On the contrary, Fig. 6 shows that increasing the number of energy groups introduces additional complex branches, whose number and disposition are related to the group boundaries adopted to collapse the cross sections: the CASMO-4 and CASMO-7 grids (see Table 1) share the same fast and epithermal groups, while the CASMO-4 and the CASMO-2 grid are featured by the same thermal group. As a consequence, the branches associated with the shared groups overlap. The location of the branches is related to the group-wise mean collision frequency, $\ell^{-1}_{g,coll} = v_g \Sigma_{g,t}$, indicated by the dashed lines. In case G → ∞, the eigenvalues would continuously fill the plane defined by $Re(\omega) < -min(\ell^{-1}_{g,coll})$. The complex branches are also strongly influenced by the angular approximation order employed, as visible from Fig. 7, which helps to understand the interplay between the angle and energy variables. Each energy group generates a batch of eigenvalues whose spread increases for larger values of $Im(\omega)$. As observed in Abrate et al. (2021a,b), the

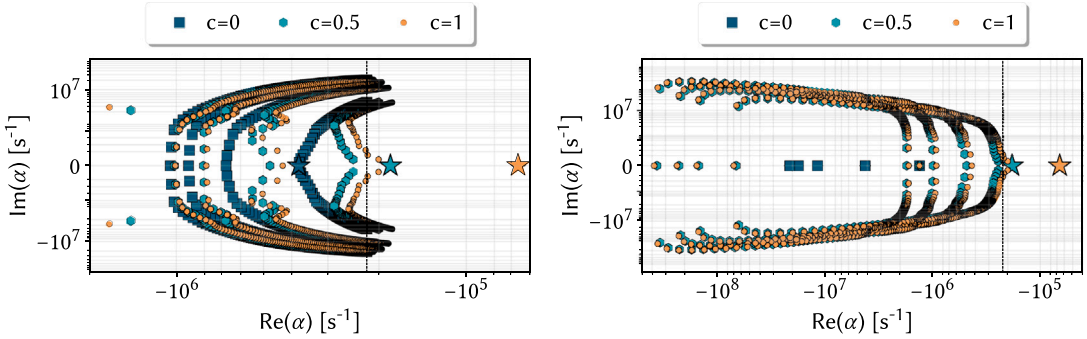


Fig. 8. Prompt spectrum (α) of a homogeneous slab considering isotropic scattering, computed with P_7 (left) and S_8 (right) models (N_x = 100, G = 1). For the sake of readability, the ordinate axes of the graphs are linear in the interval $[-5\times10^5, 5\times10^5]$.

batch in each group is formed by N + 1 (or N) symmetric, wing-shaped branches, where N is the odd (or even) order of the P_N (S_N) mode. New branches appear only when the succeeding odd/even order for the P_N/S_N model is employed, while even (or odd) values of N (or N + 1) only induce some distortions of the spectrum shape. The symmetry of the branches with respect to the real axis is due to the symmetry of the roots of the Legendre polynomial.

The mutual disposition of the wing-shaped branches depends on the interaction between neutrons and the diffusing medium. Fig. 8 shows the time spectrum of the one-group P_7 and S_8 models for a non-multiplying medium featured by different values of secondaries per collision $c = \Sigma_s/\Sigma_t$. In the P_7 case, each angular batch is independent for $c = 0$, due to the absence of scattering, which couples the directions. When scattering is triggered, repulsion and crossing between the branches are evident, due to the collision-driven angular redistribution. In a multi-group case, the same physical justification can be adopted for each group.

The S_8 model exhibits the same behaviour, with some notable exceptions. First, in the case of a purely absorbing medium, $c = 0$, the α spectrum degenerates into five points, and no fundamental mode can be distinguished. This is a consequence of the inherent structure of the S_N model, which decouples each direction in the case of a purely absorbing medium, contrarily to the P_N model. The five degeneracy points should be interpreted as one degeneracy per each $N/2 = 4$ direction, due to the symmetry of the quadrature weights, plus one degeneracy associated with the Mark boundary conditions. In this case, it is not possible to identify a fundamental eigenvalue. When c increases, the spectrum becomes similar to the P_7 case, but with the wing-shaped batches pointing towards $-\infty$. The difference between the P_N and S_N spectra cannot be ascribed only to the differences in their numerical setup, but also to the absence of fission and external source. In case fission is introduced, the two angular models would provide similar time spectra.

Figs. 9 and 10 show some details of the time spectrum for the three material configurations discussed previously. The time spectra are computed for a one-group, P_7 model (Fig. 9), with the purpose of highlighting the angular behaviour in the presence of heterogeneity, and for a two-group, P_3 model (Fig. 10), aiming at evaluating the energy effects. The shape of the bare reactor spectrum is consistent with the previous observations. When the heterogeneity appears, the pattern becomes more intricate because of the interplay of spatial, angular and energy effects. The one-group case is featured by N + 1 (i.e., 8) slightly overlapping branches per imaginary half-plane for both the heterogeneous arrangements, in contrast with the 4 branches per each half-plane for the homogeneous reactor. Since both configurations have different numbers of layers but are both featured by water and fuel, the number of complex branches turns out to be proportional to the number of materials. The number of layers seems to affect only the disposition and separation of the branches, as observed in Fig. 8. At a first glance, the fact that the angular branches are sensitive to the material properties could appear non-physical, since $\hat{L}\phi = \vec{\nabla}\cdot(\vec{\Omega}\phi)$. Hence, this phenomena most likely origins from a spatial-angular effect, in analogy to the spatial-energy coupling that features the heterogeneous media (Weinberg and Wigner, 1958) and that can be observed in Fig. 10, where two details of the spectrum around $-\ell^{-1}_{1,coll}$ (fast) and $-\ell^{-1}_{2,coll}$ (thermal) are provided: the fast and the thermal branches for the heterogeneous media exhibit different shapes, justified by spatial, angular and energy effects (see Fig. 9).

The influence of the criticality level on time spectra can be appreciated with Fig. 11(a), where the ω-spectrum computed with 25 meshes and the P_1 model collapsing the cross sections on the CASMO-4 grid is reported for a linearly anisotropic, fissile slab. As it can be noticed, the fundamental eigenvalue exhibits a large sensitivity to the criticality level, making its numerical search quite challenging in practice, especially when ω_0 falls in the interval $[-\lambda_1, 1]$.

Contrarily to the γ case, the number of complex branches in the time spectrum seems independent of the energy spectrum $\varphi(E)$ featuring the system, as it can be deduced from Fig. 11(b). Another relevant information can be obtained comparing these spectra with the one represented in Fig. 6, computed with the same N_x and N but using the CASMO-7 grid. In the last case, most of the groups are thermal, while the 8 groups employed for the cases in Fig. 11(b) are almost uniformly spaced in lethargy. The differences in the grids are reflected by the distribution of the frequencies, which are more evenly distributed in the 8-group case with respect to the CASMO-7 case, where most of the branches are located towards the thermal collision frequencies.

3.4. The density eigenvalue

Except for ω, both k and γ act on the number of particles emitted by fission and scattering, respectively, despite these parameters cannot be modified, in practice, without affecting also other parameters. Probably inspired by the desire of avoiding this drawback, Ronen et al. (1976) introduced the so-called *density* eigenvalue,

$$\hat{L}\varphi_{\delta,n} = \frac{1}{\delta}\left(\hat{S} + \hat{F} - \hat{R}\right)\varphi_{\delta,n}, \tag{16}$$

which can be interpreted as the ratio between the number of particles interacting in the system and the number of particles leaking out of the system,

$$\delta = \frac{\langle(\hat{S} + \hat{F} - \hat{R})\varphi_{\delta,n}\rangle}{\langle\hat{L}\varphi_{\delta,n}\rangle}. \tag{17}$$

This eigenvalue lends itself to two physical interpretations. The most intuitive one is to consider δ as a scaling factor for the material density. From a different perspective, under some assumptions it can be interpreted as a *streaming* eigenvalue changing the relationship between the angular flux and the angular current ($\hat{\Omega}\phi$). In this respect, δ scales the geometrical size of the system (Velarde et al., 1978; Perel et al., 1999). With respect to what it can be found in the literature, this equivalence condition actually holds only with a specific assumption:

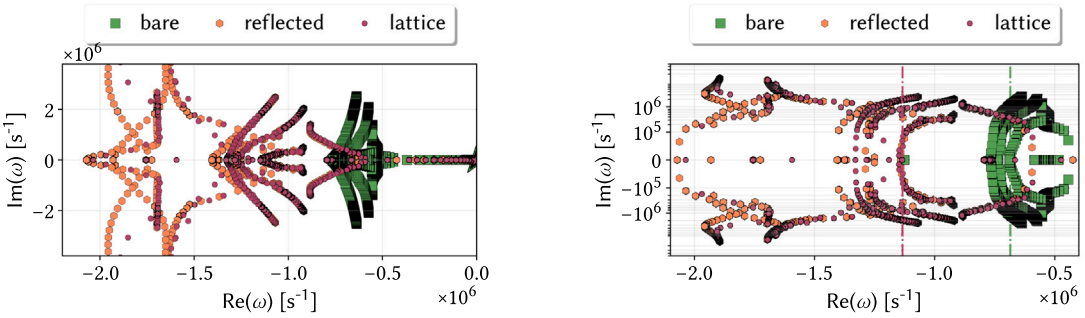


Fig. 9. Time spectrum (left) a detail of the same spectrum (right) for $\mathrm{Re}(\omega) = [-2 \times 10^6, -5 \times 10^5]$ ($N_x = 121$, P_7, G = 1).

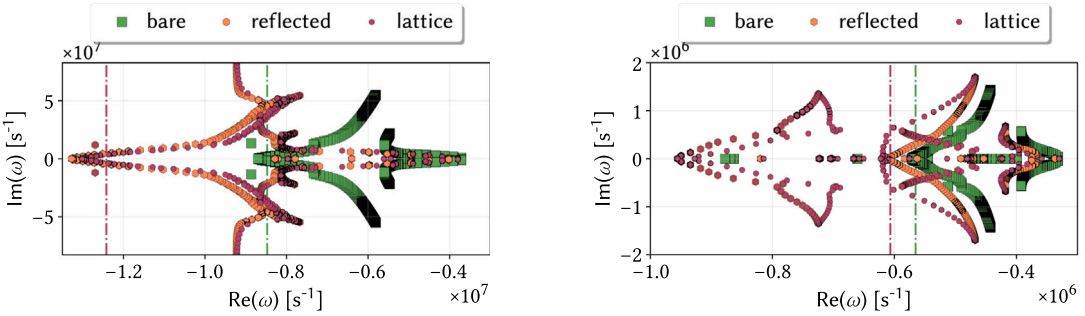
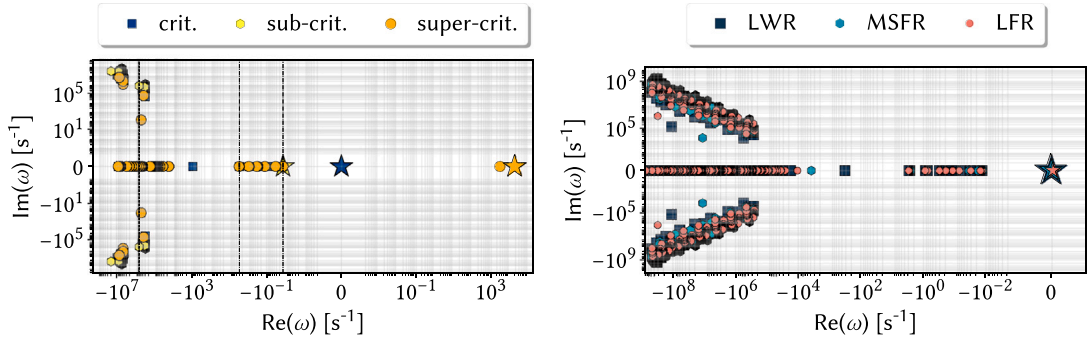


Fig. 10. Details on the fast (left) and thermal (right) frequencies featuring the time spectrum ($N_x = 121$, P_3, CASMO-2).



(a) $N_x = 25$, P_1, *CASMO-4*. (b) $N_x = 25$, P_3, *G=8*.

Fig. 11. Time spectra for homogeneous, fissile slabs considering linearly anisotropic scattering. The dashed black line indicates the Corngold limit (left) and the delayed spectrum limits ($-\lambda_R$ and $-\lambda_1$).

if each geometrical coordinate is scaled with a factor β, $\vec{\mathcal{R}} = \beta\vec{r}$, the divergence of the current should scale accordingly,

$$\begin{aligned}\nabla \cdot (\vec{\Omega}\phi(\vec{r}, E, \vec{\Omega})) \longrightarrow & \beta\nabla \cdot (\vec{\Omega}\phi(\vec{\mathcal{R}}, E, \vec{\Omega})) \\ & = \beta(\vec{\Omega} \cdot \nabla\phi(\vec{\mathcal{R}}, E, \vec{\Omega}) + \phi(\vec{\mathcal{R}}, E, \vec{\Omega})\nabla \cdot \vec{\Omega}).\end{aligned} \tag{18}$$

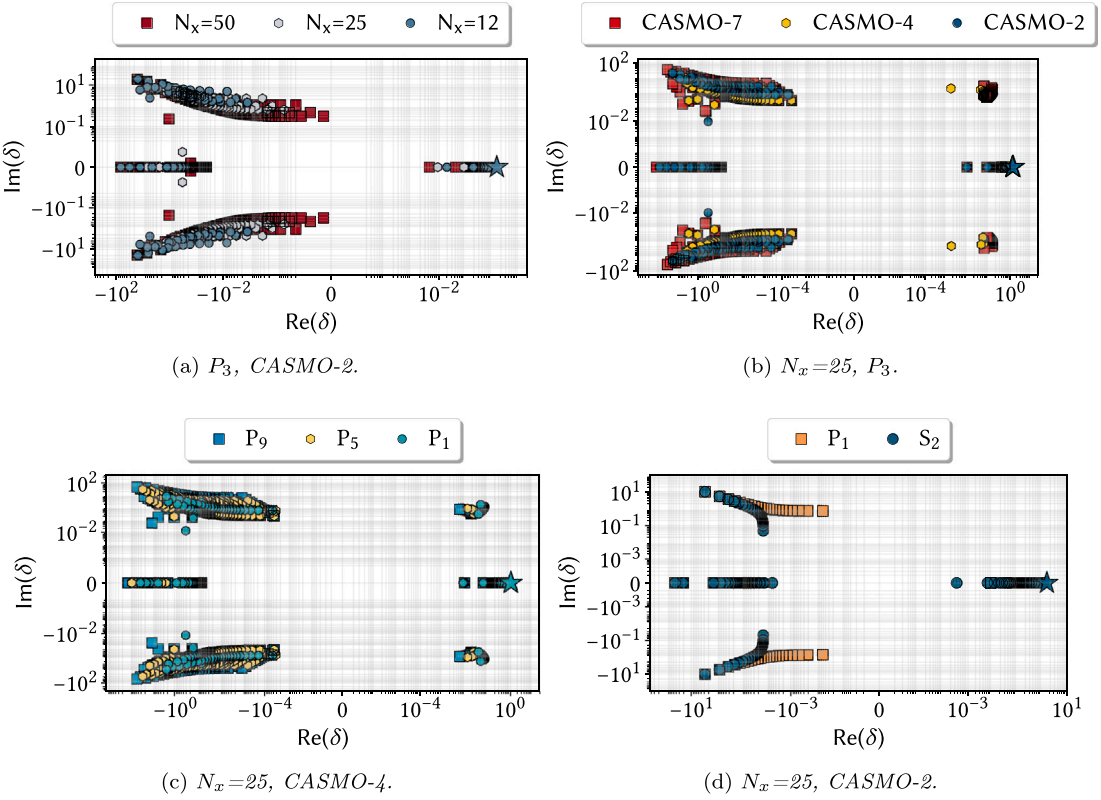
It can be shown that this condition is satisfied whenever $\nabla \cdot \vec{\Omega} = 0$. When the reference frame is not fixed in space, as for curvilinear geometries (Bell and Glasstone, 1970), the condition expressed in Eq. (18) should be examined case by case. For spherical and cylindrical frames, it is possible to prove that this condition still holds. For other geometries, a useful generalisation of the scattering term can be found in Pomraning (1989).

When $\beta = 1/\delta$, the scaled system is critical, as δ cancels out in Eq. (16): given a certain material composition with $k_\infty > 1$, criticality is attained by changing the surface-to-volume ratio of the system, and, thus, the leakage term. The condition on k_∞ can be deduced from elementary criticality theory in diffusion: for a homogeneous, one-speed slab with zero-flux boundary condition δ_n reads

$$\delta_n = \frac{\sqrt{k_\infty - 1}}{LB_n}, \tag{19}$$

which yields a real and positive eigenvalue if and only if $k_\infty > 1$. This simple example also shows that $\delta_0 \to \infty$ when $B_0 \to 0$: it is not possible to derive a δ-based criticality condition for the infinite medium, where no leakage occurs by definition.

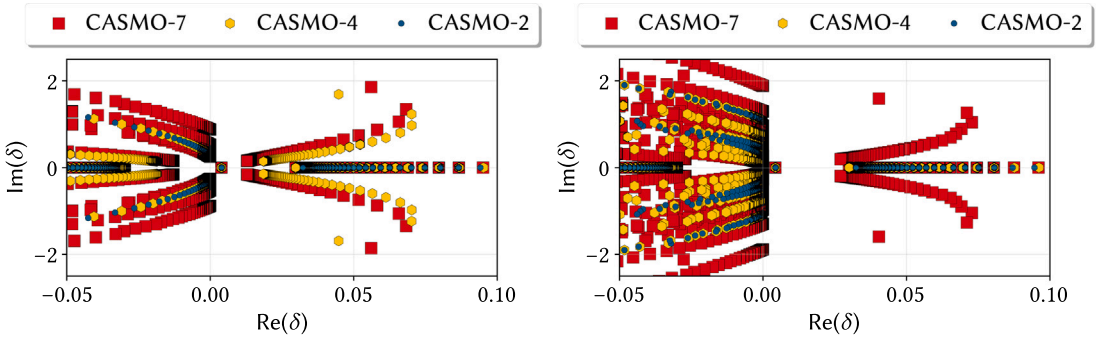
Fig. 12 helps to understand the general structure of the δ-spectrum, which appears constituted by a branch of strictly real and positive eigenvalues, a branch of strictly real and negative eigenvalues and two complex conjugate branches. Additional DoF introduced by larger values of N_x do not alter the overall shape of the spectrum, adding more eigenvalues towards the origin of the complex plane, while increasing N and G generates a number of complex branches that is proportional to both N and G: two complex conjugate branches appear in the P_1, CASMO-2 case (Fig. 12(d)), six complex conjugate branches are present for the P_3, CASMO-2 case (Fig. 12(b)), six branches can be appreciated for the P_1, CASMO-4 case (Fig. 12(c)), while twelve branches can be



(a) P_3, *CASMO-2*. (b) N_x=*25*, P_3.

(c) N_x=*25*, *CASMO-4*. (d) N_x=*25*, *CASMO-2*.

Fig. 12. δ-spectrum for a homogeneous, fissile slab considering isotropic scattering.



(a) $N_x = 50$, P_1. (b) $N_x = 50$, P_3.

Fig. 13. δ-spectrum for a homogeneous, fissile slab with isotropic scattering.

observed for the P_3, CASMO-4 case (Fig. 13(b)). The position of the complex branches is strongly related to angular-energy effects, which cannot be appreciated in the case of the k eigenvalue, since fission is isotropic. The P_1, CASMO-4 model (Fig. 13(a)) is featured by two complex branches with Re(δ)> 0, while, if the same system is solved with P_3 and the CASMO-4 grid (Fig. 13(b)), these branches can be found in the Re(δ)< 0 half-plane.

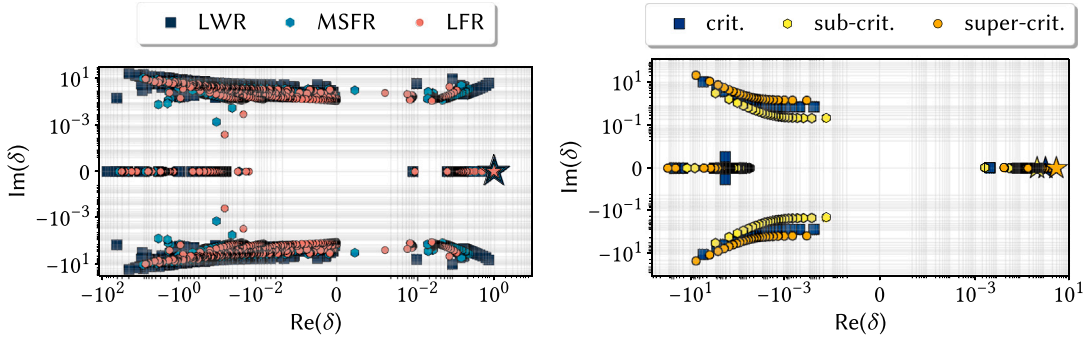
Finally, it is interesting to highlight that, when even-order (odd-order) P_N (S_N) approximations are employed, a set of extremely large eigenvalues ($\sim 10^{15}$) appears. These spurious eigenvalues stems from the fact that $\hat{L}$ becomes singular when such parity orders are employed. The S_N formalism is useful to give a physical interpretation to this effect. When N is odd, the following equation could be written for the streaming direction $\mu_{N/2+1} = 0$, parallel to the slab boundaries,

$$\mu_{N/2+1} \frac{\partial \phi(x, \mu_{N/2+1})}{\partial x} = -\frac{1}{\delta} \Sigma \phi(x, \mu_{N/2+1}) = 0. \tag{20}$$

Since Σ and ϕ are non-zero, Eq. (20) holds only in the limit case $\delta \to \infty$.

As visible in Fig. 14, the overall shape of the spectrum seems not very sensitive neither to the energy spectrum featuring the system nor to the offset from criticality, provided that criticality can be achieved with δ. In this respect, it is not always possible to justify the existence of a positive, real eigenvalue, especially in the case of a heterogeneous medium. The cases with $\delta_0 < 0$ seem to suggest that criticality can be attained by exchanging artificially the rôle of production and removal terms in case the fissile material was not sufficient to sustain the chain reaction (as discussed previously for the homogeneous, one-speed diffusion case). This behaviour should not be regarded as an unpleasant issue concerning δ, but rather as a consequence of the additional physical constraints considered in the search for criticality. Fig. 14(b) also shows that, among the "static" eigenvalue formulations, δ_0 is the most sensitive one to the offset from criticality.

Finally, Fig. 15 shows the effect of the spatial heterogeneity on the spectrum shape. In this case, apart from additional complex branches around $Re(\delta) = 0$, related to the use of more energy groups and common to each arrangement, it is not possible to appreciate evident



(a) $N_x = 25$, P_3, $G{=}8$. (b) $N_x = 25$, P_1, *CASMO-2*.

Fig. 14. δ-spectrum for homogeneous, fissile slabs with linearly anisotropic scattering.

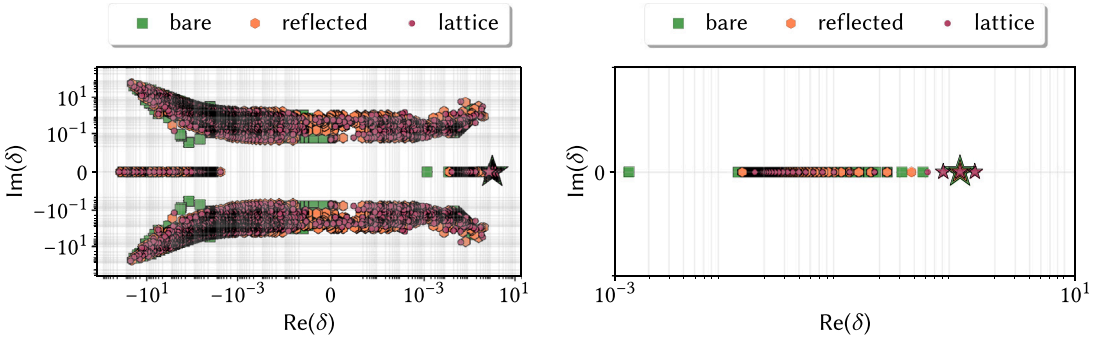


Fig. 15. δ-spectrum (left) for three critical slabs featured by different material arrangements (N_x = 121, P_3, CASMO-7) and an enlargement on the positive half-plane (right).

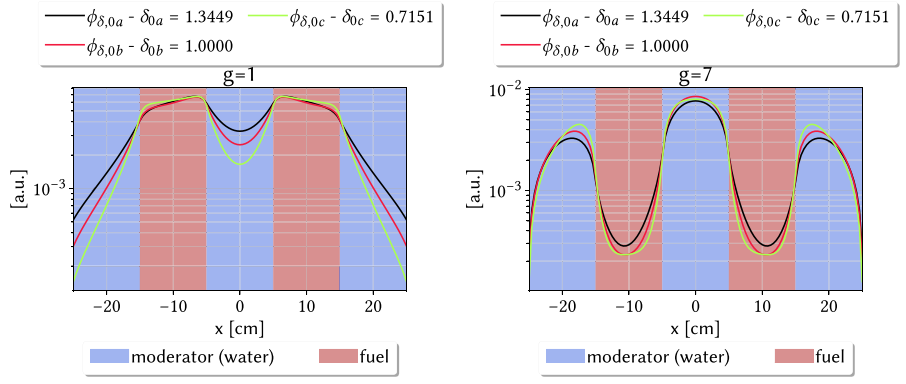


Fig. 16. Group-wise fundamental δ modes obtained for a heterogeneous, moderated, critical system.

deformations of the spectrum due to the number of layers or their composition. Nevertheless, the detail of the real, positive branch reveals more fundamental eigenvalues for the lattice case, each associated with an eigenfunction with uniform sign. These fluxes, reported in Fig. 16, are very similar in space but featured by different energy spectra. Also these multiple fundamental eigenpairs are related to the competition between production and removal and between fuel and moderator.

3.5. Summary on the analysis of the eigenvalue spectrum

In the previous sub-sections, the behaviour of the eigenvalue spectrum has been thoroughly studied with respect to both modelling and physical parameters, trying to highlight general features of its shape that can be relevant for different applications, encompassing, for instance, the optimisation of numerical solvers and higher-order perturbation analysis. In order to support the reader, the results and observations made in the previous subsections are summarised in the following.

The characteristics of the eigen-spectrum mostly depend on the specific physical term that is modified in the balance equation by the introduction of the eigenvalue. For a given eigenvalue problem, the shape of the spectrum is determined by the numerical model adopted to approximate the transport equation (N_x, N, G) and by the physical features of the system (the reactor design, the spatial arrangement, the anisotropy of the scattering...):

- multiplication eigenvalue k: the spectrum is always real. While the numerical approximations do not significantly affect the spectrum shape, the off-criticality, the angular model (S_{N+1} vs. P_N) and the spatial arrangement modify the separation and disposition of the higher-order eigenvalues.
- collision eigenvalue γ: the spectrum is composed by a set of purely real eigenvalues and by possible complex eigenvalues, which are mostly introduced by energy and directional effects.

Table 3
Summary of the sensitivity of the spectrum to modelling and physical parameters (H = high sensitivity, I = intermediate sensitivity, L = low sensitivity).

	N_x	N	G	Anisotropy	Energy spectrum	Heterogeneity	Angular model	Off-criticality
k	L	L	L	L	L	H	I	I
γ	L	I	I	H	H	I	I	H
ω (α)	L	H	H	L	I	H	H	I
δ	L	H	H	L	I	L	I	L

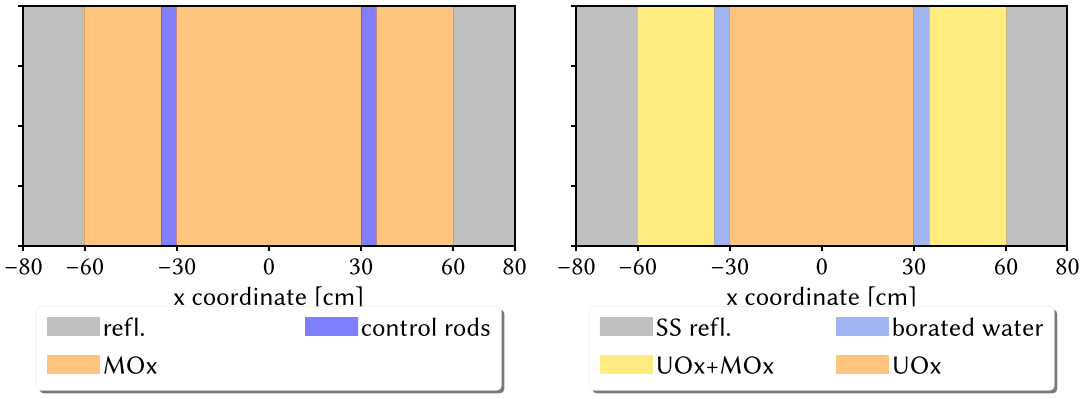


Fig. 17. One-dimensional models of the LFR-like core (left) and LWR-like core (right) used for the sensitivity analysis.

The spatial discretisation does not alter its shape, while the order of the angular model, the anisotropy of the scattering and the number of energy groups strongly modify the disposition of the higher eigenvalues. Also the reactor energy spectrum and the off-criticality level are important parameters for determining the shape of the eigenvalue spectrum.

- time eigenvalue ω: the spectrum exhibits real discrete eigenvalues and a set of eigenvalues which asymptotically ($N_x \to \infty$, $N \to \infty$, $G \to \infty$) constitute a *continuum* on the complex plane. The position of the discrete terms depends on the presence of delayed emissions in the model and on the off-criticality level, while the energy model and the order of the angular approximation affect the way in which the eigenvalues progressively fill the *continuum* part. The complex branches align according to the group-wise collision frequency, and their number is proportional to the quadrature set used in the angular model. Another relevant parameter for the spectrum shape is the spatial heterogeneity, which introduces frequencies that are representative of the different materials.
- streaming/density eigenvalue δ: the spectrum is composed by a set of purely real eigenvalues and by complex branches related to energy and directional effects. Despite its complicated structure, the shape of the δ spectrum is not as sensitive as the ω spectrum to the spatial heterogeneity and to the angular model. However, the number and the position of the complex branches are heavily affected by N, and extremely large eigenvalues may appear in the P_N (S_{N+1}) model when N is even. In heterogeneous systems, more than one dominant eigenvalue could be found.

Table 3 briefly summarises the impact of different modelling and physical parameters on the spectrum of each eigenvalue formulation.

4. Sensitivity of the energy spectrum on the eigenvalue formulations

The second part of the work is devoted to performing a sensitivity analysis of the energy spectra computed with the eigenvalue problems analysed previously with respect to the critical spectrum of a reference system. A similar analysis has been already carried out in Cacuci et al. (1982), although only for a thermal, reflected slab, described with a two-group S_4 model. In the reference, the critical spectrum of the system was compared with the spectra $\varphi_x(E)$ ($x = k, \gamma, \delta, \omega$) computed solving the eigenvalue problems for slightly off-critical systems. The departure from criticality was assumed to stem from perturbations in the input parameters (e.g., the core dimensions or the fission cross section). The outcomes of the analysis carried out in the reference highlighted the features of the eigenvalue formulations from a more practical point of view, and could be summarised as:

- a qualitative analysis related to the spectra hardness in the core and reflector was established through local spectral indexes, showing that the spectra hierarchy in each region holds independently on the physical parameter inducing the deviation from criticality;
- a quantitative analysis showed that the relationship between the critical spectrum $\varphi_{k=1}(E)$ and $\varphi_x(E)$ ($x = k, \gamma, \delta, \omega$) depends on the physical parameter responsible for the deviation from criticality, implying that an eigenvalue formulation yielding a spectrum that is always the closest to the critical spectrum does not exist. When the deviation from criticality was caused by a uniform change in the dimensions (which is a rather unlikely situation, in practice), $\varphi_\delta(E) = \varphi_{k=1}(E)$, while when a physical parameter related to fission was perturbed, $\varphi_k(E)$ is the closest spectrum to the critical one. In every situation, $\varphi_\gamma(E)$ had intermediate features compared to other spectra, suggesting that it is the most appropriate one to describe the reference system when the deviation from criticality is not related to fission.

In this section, we try to enrich the analysis carried out in Cacuci et al. (1982), considering also a fast system based on the LFR concept, with the aim of drawing more general conclusions. In addition to perturbations in some physical parameters, our work focuses also on temperature effects and perturbations in the computational model, like boundary conditions and scattering anisotropy order. The outcomes of this study should provide some empirical insights that may support the choice of the most appropriate eigenvalue formulation for reactor physics applications, like the preparation of group constants and the calculation of kinetic parameters.

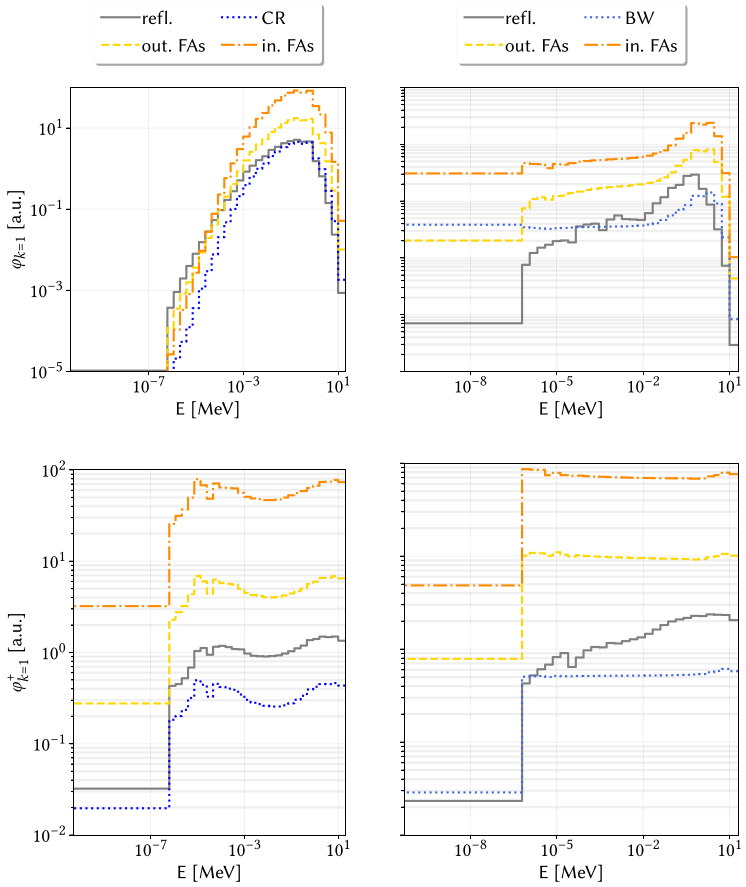


Fig. 18. Direct (top) and adjoint (bottom) critical energy spectra in the regions of the LFR (left) and LWR (right) cores depicted in Fig. 17 ($N_x = 99$, P_7, $G = 29$).

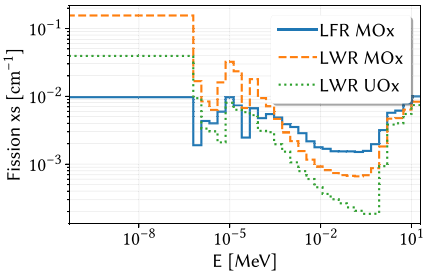


Fig. 19. Fission cross section for the reactor configurations considered in this section.

The accuracy of the group constants depends on the group structure (i.e., number of groups and their boundaries) and on the spectrum used for the collapsing. For design calculations, the most appropriate spectrum is the critical one, $\varphi_{k=1}(E)$. However, due to modelling and input data uncertainties, the spectrum used in the collapsing process is an approximation to $\varphi_{k=1}(E)$. As concluded in Cacuci et al. (1982) and remarked in the following, the closest eigenvalue spectrum to $\varphi_{k=1}(E)$ depends, in general, on the parameter causing the deviation from criticality. Each eigenvalue formulation tunes one or more terms of the neutron transport equation to satisfy the balance: when the tuning parameter (i.e., the eigenvalue) acts in "the opposite direction" of the perturbation altering the criticality, its spectrum tends to the critical one.

Fig. 17 sketches the two one-dimensional slab models for the LFR and LWR cores devised for this study. The rationale behind the choice of these systems is to have a relatively simple but representative heterogeneous arrangement, featured by central and peripheral fuel assemblies (FAs), the control rods and the external reflector (in the LWR case, the reflector is assumed to be made of stainless steel, as in Gen-III+ reactors). The multi-group cross section characterising these systems have been generated with the Serpent 2 Monte Carlo code (Leppänen et al., 2015) on a 29-group structure consisting of one fast group, one thermal group and 28 groups with equal lethargy widths between $6.25 \cdot 10^{-07}$ and 10 MeV. This energy grid has been conceived to allow a consistent comparison between the fast and thermal energy spectra featuring the systems.

The forward and adjoint critical spectra in the different regions composing these two systems are represented in Fig. 18. The adjoint spectrum has the same hierarchy in the regions of both systems, consistently with the interpretation of the adjoint as "importance" density function (Lewins, 1965): the most important neutrons are located in the central FAs, followed by the peripheral FAs, the reflector and the control region. In the LWR the adjoint spectrum is approximately uniform above the thermal region, except for the reflector, where the importance is roughly inversely proportional to E, while in the LFR the adjoint has two local maxima, in correspondence of the maxima of the fission cross section for the LFR FAs (see Fig. 19).

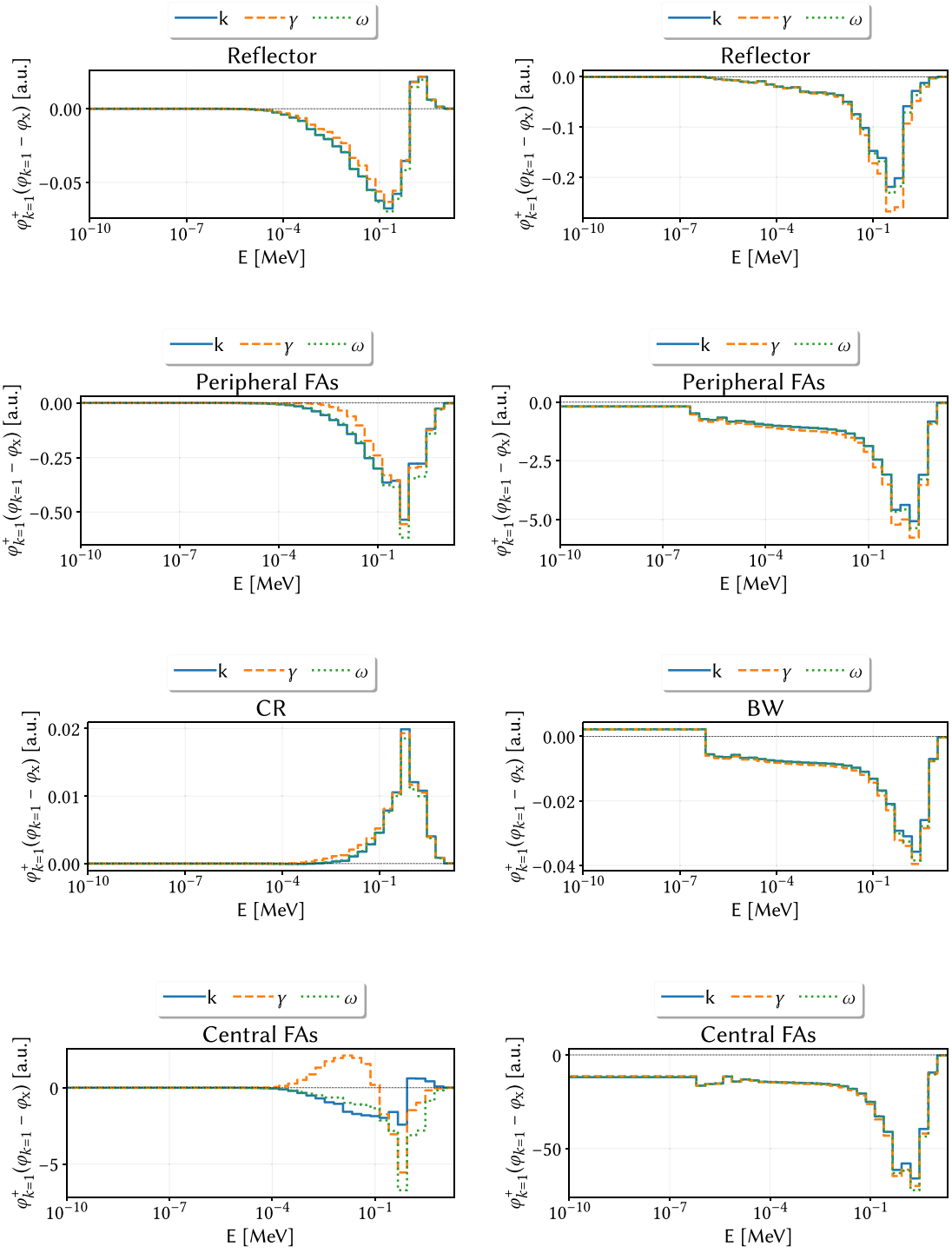


Fig. 20. Relative difference between the critical spectrum $\varphi_{k=1}$ (N_x = 344, P_1) of LFR (left, k_{eff} = 1.00256) and LWR (right, k_{eff} = 1.00596) cores and the spectra of the same system but computed with N_x = 64.

4.1. Effect of spatial meshing

The first model perturbation studied involves the adoption of a coarser spatial mesh. The "sensitivity" of the eigenvalue energy spectra is assessed considering, in each spatial region i, the difference between the critical spectrum (computed, in this case, with a P_1 model and N_x = 344 meshes) and the spectrum associated with each eigenvalue formulation, weighted with the adjoint spectrum of the critical system,

$$\varepsilon_{x,i,g} = \varphi^{+}_{k=1,i,g}(\varphi_{k=1,i,g} - \varphi_{x,i,g}) \qquad x = k, \gamma, \delta, \omega. \tag{21}$$

This adjoint-based metrics is preferred to the standard relative error to avoid shifts in the energy profile of the relative difference. As an example, in the LFR the differences in the thermal and low epithermal regions would be weighted more than the ones affecting the high epithermal and fast region, despite their lower "importance". Thus, to prevent the relative error masking the behaviour of the energy spectra, the adjoint flux integrated on each region is used. Despite the adoption of the adjoint flux, it should be noticed that Eq. (21) is not derived from classical perturbation analysis, but it is a rather intuitive and simple way of measuring the sensitivity of the energy spectrum.

The adjoint-weighted errors for the k, γ and ω eigenvalues are visible in Fig. 20. Apart from the central FAs region, the errors have a similar trend for each formulation in the LFR case. The γ formulation is the least sensitive to N_x in the outer regions, while in the CR and in the central FAs k is the most accurate. In the LWR case the errors have a more regular behaviour, having the same energy profile in each region and preserving the accuracy ranking (k, ω and then γ). The δ eigenvalue has been analysed but omitted from the figure because of its nature: being tightly related to neutron leakages, the adoption of a coarser mesh clearly introduces large distortions in the leakages, due to the poorer representation of the flux gradients, which in turn generates very large errors.

4.2. Effect of angular model

The effect of perturbations in the angular model on the spectra can be appreciated in Fig. 21, where the critical spectrum computed with a P_7 model is compared to the ones obtained with a P_3 model.

In both reactors, the weighted, group-wise error is maximum in the fast region. For the LFR, the trend with respect to E is the same in the outer regions of the core, where the eigenvalue spectra are harder than the critical spectrum, while in the innermost FAs the error changes sign, similarly to what observed in Section 4.1 for the spatial meshes. The negative sign in the outer regions indicates a spectrum hardening. The energy spectra computed with the different eigenvalues can be hardly distinguished. Similar considerations can be made also in the case of P_5 and P_1 models, suggesting that the various spectra are equally sensitive to the angular model, for a fast reactor.

In the LWR case the trend with respect to E is similar for all regions (i.e., the eigenvalue spectra are softer than the critical spectrum), except for the borated water layer, where the eigenvalue spectra are harder. In this case, a certain discrepancy between δ and the other eigenvalue formulations can be appreciated. The larger sensitivity of δ can be due to the impact of the angular model on the scattering with the moderator, which has a direct impact on leakages. Similar considerations hold also when the calculations are carried out with P_5 and P_1 models.

4.3. Effect of scattering anisotropy

The order of the scattering anisotropy L is a parameter that, with the optical thickness of a system, marks the difference between transport models and diffusion, which is not able to account for values of $L > 1$. Fig. 22 shows the usual sensitivity indicator for the eigenvalue formulations. To better appreciate the trends of these differences in the various regions, the average cosine of the scattering angle μ_0 has also been reported as a function of E. The trend of $\mu_0(E)$ is approximately the same across the LFR regions, i.e. almost 0 in the thermal and epithermal regions and forward-peaked in the fast region. In the LWR, $\mu_0(E)$ exhibits important differences moving towards the centre of the core: in the reflector it behaves like in the LFR case, while in the borated water layer and in the peripheral and central FAs the scattering is forward-peaked also in the epithermal region, due to the presence of hydrogen.

The trend of the adjoint-weighted error between the critical spectrum and the ones computed with the eigenvalue formulations is approximately the same for the reflector, control rod and peripheral FAs in the LFR: the eigenvalues behave similarly, but δ is the most appropriate formulation. Neglecting the forward-peaked scattering at high energy globally softens the eigenvalue energy spectra ($\varphi_{k=1} < \varphi_x$): the isotropic scattering increases the chances of high-energy neutrons to stay in the same region and slow down. The reduction of neutron leakages is almost counterbalanced by δ, which scales the geometry down minimising the perturbation in the energy spectrum with respect to the other formulations. The δ spectrum is the most appropriate also in the central FAs, while the error of k is shifted with respect to the one of γ and ω. The presence of a spectral shift in this region can be explained by its larger thickness: particles have more chances to stay in the central FAs, so their interaction with matter, which is affected by the eigenvalue, makes more explicit the spectral differences.

In the LWR, which is optically larger, the trend strongly depends on the region considered. The ω, γ and k spectra have a similar behaviour, being very close except for the peripheral FAs, where the γ spectrum is the most inaccurate. This large discrepancy can be related to the position of this region, which is close to the reflector, where the effect of anisotropy on the slowing down is important. It should be also acknowledged that γ is the only eigenvalue acting directly on the terms related to the anisotropy. Since the LWR is optically larger than the LFR, the relation between anisotropy and leakage is weaker, affecting the performances of δ, which is very accurate in the borated water layer and very inaccurate in the central FAs.

In both cases, the errors generally tend to increase with energy, consistently with the behaviour of μ_0, but the LFR seems more sensitive to the anisotropy, as it can be appreciated looking at the k static reactivity.

4.4. Effect of boundary conditions

It is well known that an approximated transport model, and the related boundary conditions (BCs), cannot represent the exact physical situation, even for simple geometries, like a slab surrounded by vacuum. In the framework of the P_N approach, these BCs can be imposed with either the Mark or Marshak formalism (see Abrate et al. (2021b) for more implementation details). In this section, the perturbation induced by the adoption of the Marshak BCs instead of Mark ones is assessed for the different eigenvalue formulations.

Fig. 23 reports the results of this sensitivity study. First of all, it can be appreciated that the perturbation of BCs affects more the LFR core ($k_{\text{eff}} = 1.00039$) than the LWR one ($k_{\text{eff}} = 1.00011$): the role of the boundaries is more important in the LFR, where the mean free path is larger. This fact can be appreciated looking at the energy spectra in Fig. 23. The trend of the errors is roughly the same for the outer regions of the LFR: δ is the most inaccurate, followed by ω, k and γ. In the central FAs, γ and k are the most accurate in the epithermal and fast regions, respectively. In the LWR case it can be noticed that the errors have generally the same trend, but the δ one is always negative (i.e., it is harder than the critical spectrum), while the errors of ω, k and γ are positive in the central FAs. As expected, the sensitivity to the BCs is negligible for thermal neutrons and grows up to a maximum at the beginning of the fast region in both reactors. Boundary conditions are tightly related to neutron leakages. The P_1 model allows to relate quite intuitively Mark and Marshak BCs to different extrapolation lengths d for a bare reactor, with $d_{Marshak} > d_{Mark}$. Therefore, adopting Marshak BCs, in this case, is somehow equivalent to considering a larger reflector. At a first glance, this would suggest that δ is the best formulation in both cases, which clearly is not: δ scales either the isotopic density or the geometry of the entire domain, with a totally different impact on the spectrum.

4.5. Effect of input perturbations

The first type of perturbation in the input physical data investigated in this section is the operating temperature of the system (see Fig. 24). The LFR is critical at 673 K and becomes sub-critical when the temperature is raised up to 1073 K, while the LWR is critical at 300 K and becomes sub-critical at 570 K. In both cases, and for each region, δ is the less accurate formulation: despite the temperature affects all the material parameters (no thermal dilatation is considered) as δ does, the effect is not the same in different regions. The shape of the group-wise errors of the other eigenvalues is approximately the same for the LFR, with k and γ being the most accurate in the fast and epithermal zones,

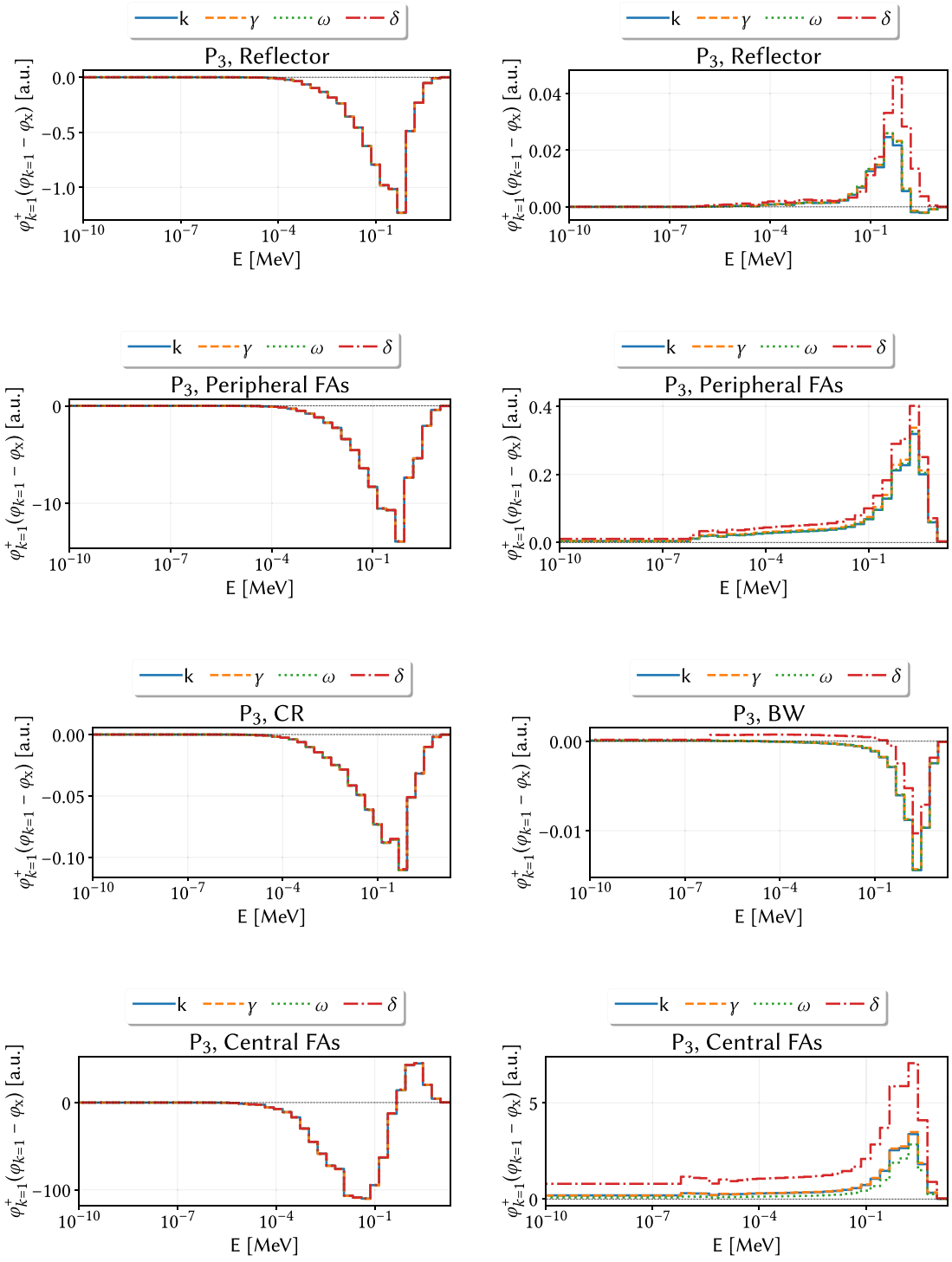


Fig. 21. Relative difference between the critical spectrum $\varphi_{k=1}$ (N_x = 140, P_7) of LFR (left, k_{eff} = 0.99973) and LWR (right, k_{eff} = 0.99985) cores and the spectra of the same system but computed with the P_3 model.

respectively. In the LWR, k seems the most accurate formulation, except for the central FAs, where γ is more accurate.

The second physical perturbation is a ±2.5% variation in the fission cross section of the initially critical reactors. According to the evidences presented in Cacuci et al. (1982), perturbations in fission-related parameters should be best represented by the k spectrum. The results for our LWR case are in line with this statement (see Fig. 26 in the Appendix), whilst the results for the LFR cases, depicted in Fig. 25, shows that this conclusion may not always hold for fast reactors: for the sub-critical case the γ spectrum is the most accurate in the outer regions, while for the super-critical case the δ spectrum is the most accurate one. The k spectrum is the most accurate in the inner regions in both cases. In the case of ± 2.5% variations in the capture cross section (see Figs. 27, 28 in Appendix), the γ spectrum is the closest to the critical one in each region of both systems, except for the central FAs of the LWR, where δ performs better.

The last two cases pertain to variations in some geometrical dimensions of the system, i.e. the thicknesses of the absorber layers and the thicknesses of the left and right reflectors. For these perturbations (see Figs. 29, 30–32 in the Appendix), the behaviour of the eigenfunctions

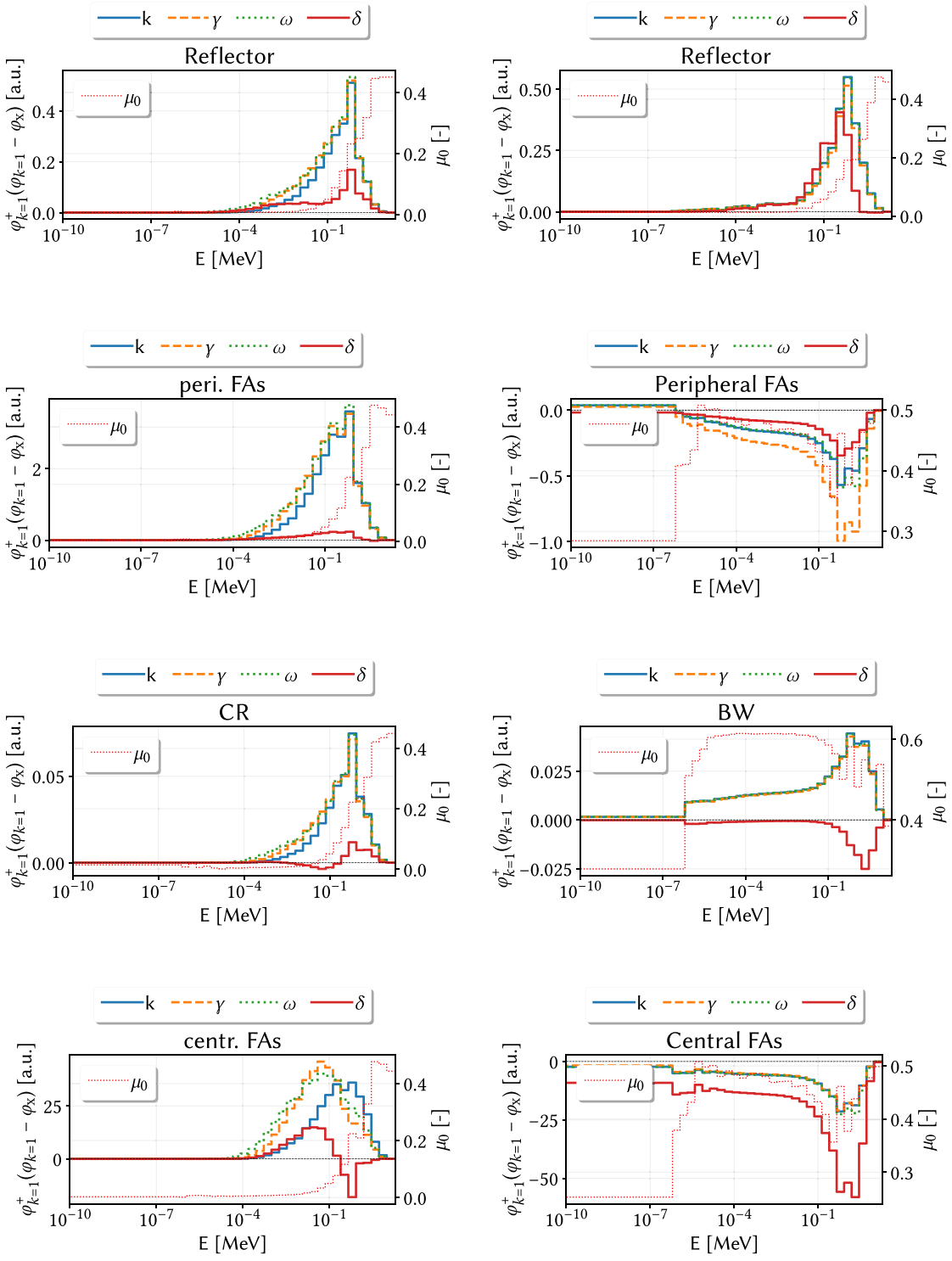


Fig. 22. Relative difference between the critical spectrum $\varphi_{k=1}$ (N_x = 140, P_3, linear anisotropy L_1) of LFR (left, k_{eff} = 1.01645) and LWR (right, k_{eff} = 1.00290) cores and the spectra of the same system but with isotropic scattering (L_0).

are strongly dependent on the reactor concept, on the spatial region and also on the energy group.

5. Conclusions and future perspectives

This paper has investigated some features of the eigenvalue and energy spectra for the most popular eigenvalue formulations arising in neutron transport, in an attempt to fill some gaps in the literature and providing useful information that can be exploited in the fields of numerical transport and reactor analysis.

The first part of the paper analyses the features of the eigenvalue spectrum on the complex plane varying both model parameters, e.g., the spatial and group meshing, and physical features, like the reactor concept and sub-criticality level. On top of its manifest importance for tuning the eigenvalue solvers, the knowledge of the shape and features of the eigen-spectrum may be very useful to interpret the

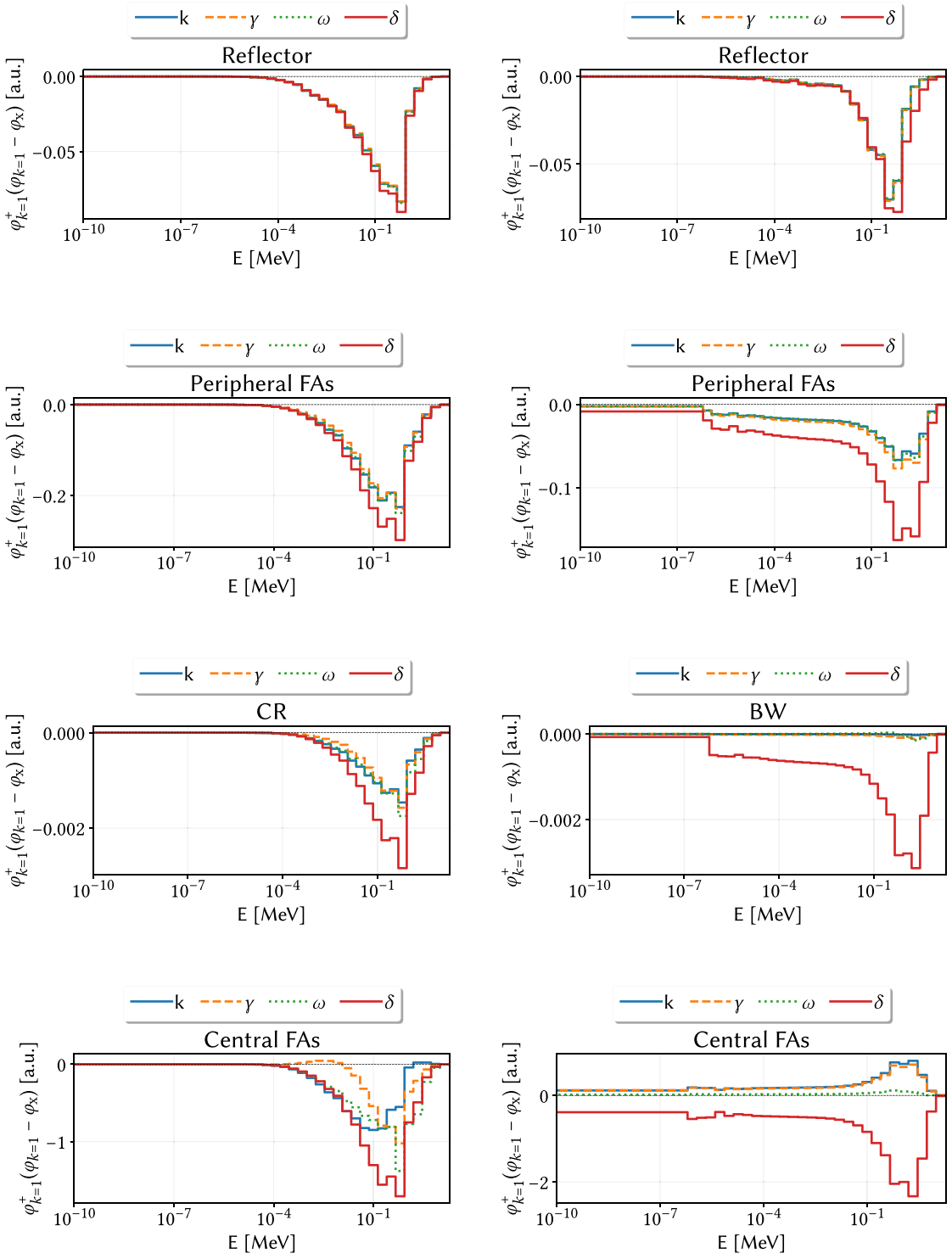


Fig. 23. Relative difference between the critical spectrum $\varphi_{k=1}$ (N_x = 140, P_1, Mark boundary conditions) of LFR (left, k_{eff} = 1.00039) and LWR (right, k_{eff} = 1.00011) cores and the spectra of the same system with Marshak boundary conditions.

effects of numerical approximations, and can support the development of methods for core stability analysis.

The second part of the paper extends previous analyses present in the literature concerning the distortion caused in the energy spectrum by the different eigenvalue formulations in off-critical systems, which is interesting for group constant collapsing and kinetic parameters generation. The departure from criticality is caused considering coarser models, e.g., poorer angular approximations and coarser meshes, and alterations in physical parameters as the scattering anisotropy and the thermodynamic conditions, which, to our knowledge, were not considered previously in the literature.

Among the outcomes of this analysis, it should be remarked that a formulation minimising the deviations from the critical spectrum

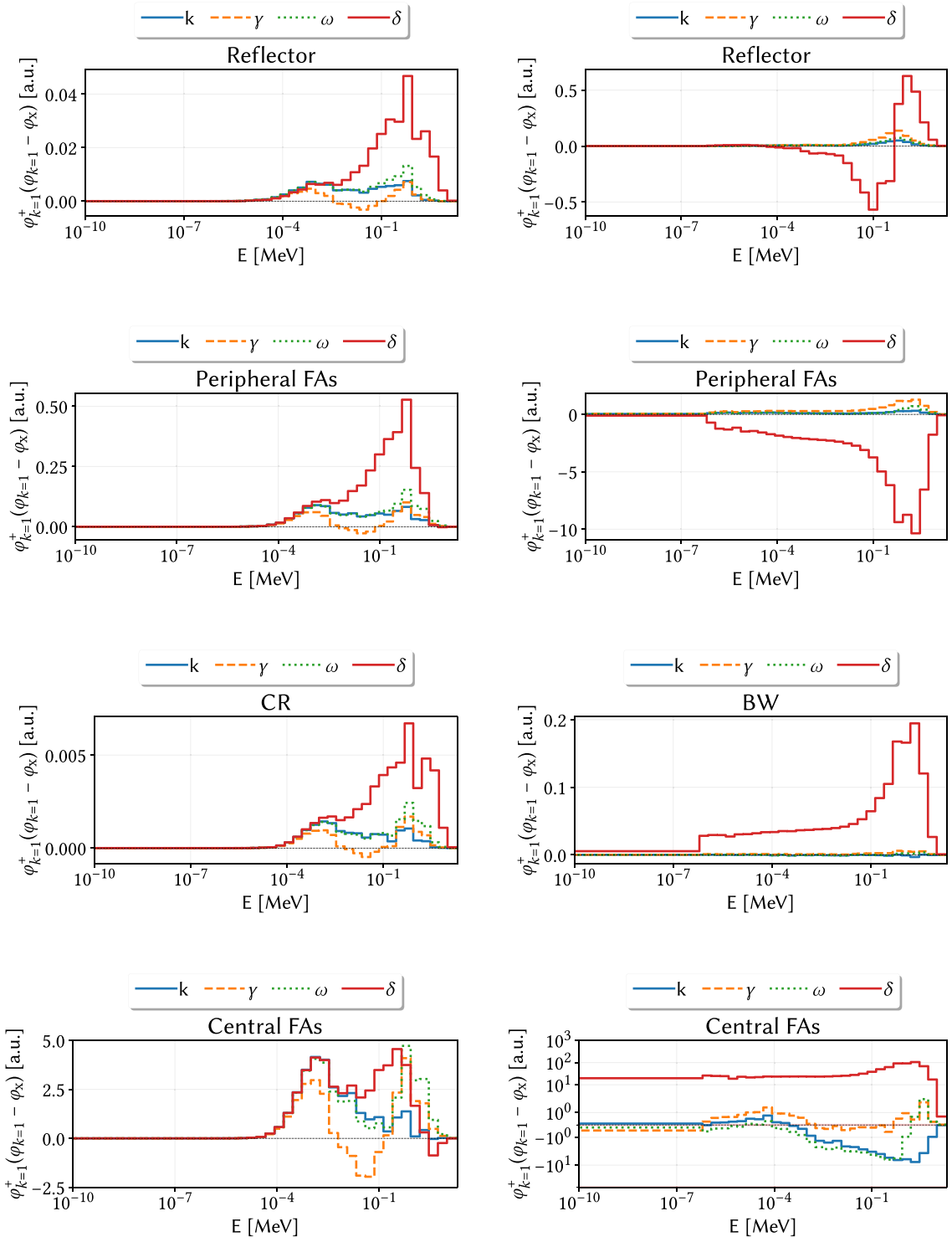


Fig. 24. Relative difference between the critical spectrum $\varphi_{k=1}$ (N_x = 140, P_1, Mark boundary conditions) of LFR (left, k_{eff} = 0.99775) and LWR (right, k_{eff} = 0.99082) cores and the spectra of the same system with higher operating temperatures (from 673 to 1073 K for the LFR and from 300 to 570 K for the LWR).

cannot be identified in general. Although deeper investigations should be carried out to obtain some more practical indications on more realistic reactor configurations, this evidence shows that the legacy approach based on collapsing the group constants on the k spectrum is usually not the most accurate one. On the contrary, γ is hardly ever the one yielding the worst results. This result, which extends the conclusions drawn by Cacuci et al. (1982) also to fast reactors, could be justified by the fact that this eigenvalue acts simultaneously on more degrees of freedom, i.e. fission and scattering, so it allows to achieve criticality with milder perturbations than the ones induced by k. As mentioned above, future works should be devoted to a more complete assessment of the eigenvalue performances, especially analysing time-dependent and more-realistic configurations, for instance involving the movement of the control rods.

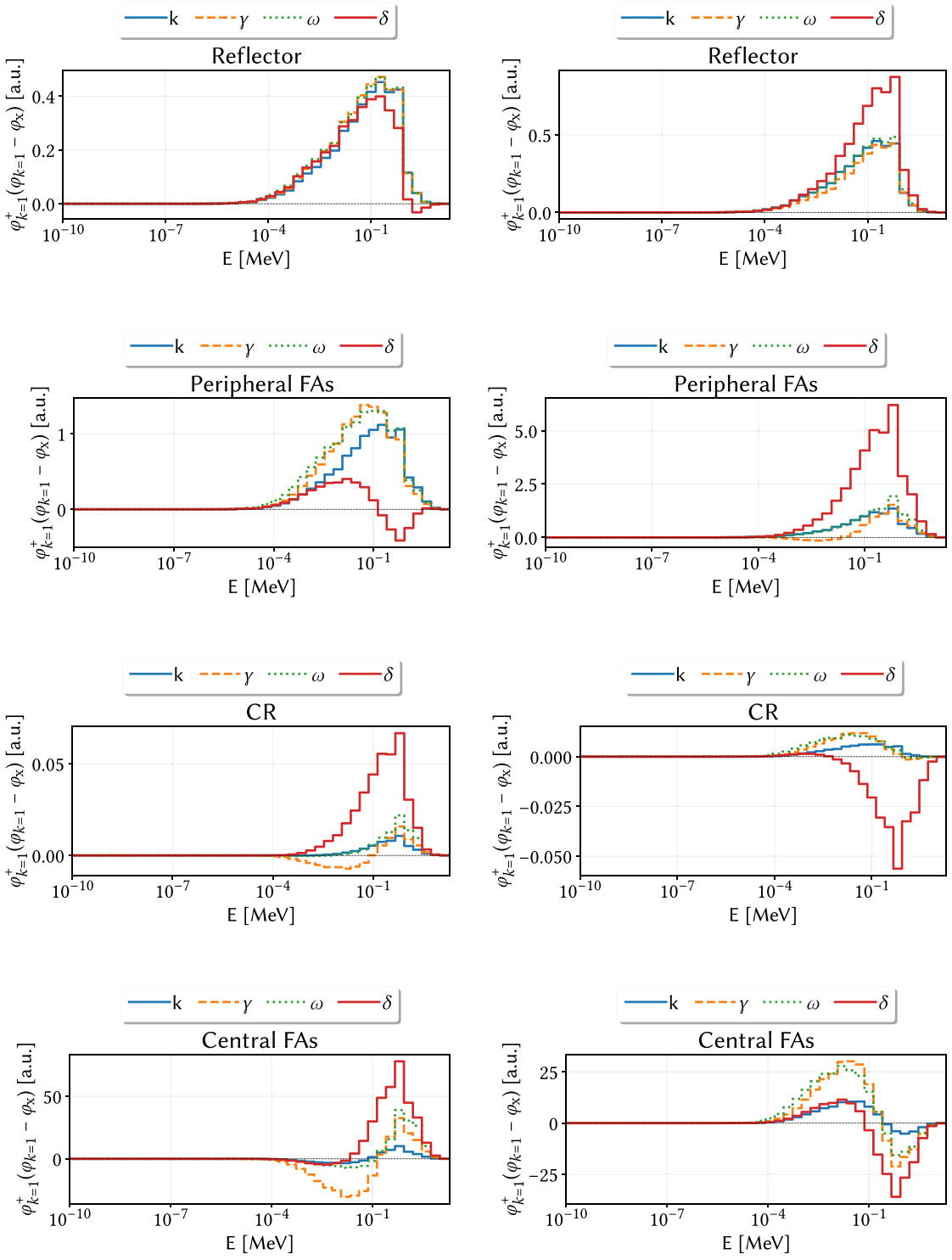


Fig. 25. Relative difference between the critical spectrum $\varphi_{k=1}$ ($N_x = 140$, P_3, Mark boundary conditions) and the spectra of the same system with higher (left, +2.5%) and lower (right, −2.5%) fission cross section for the LFR case.

Declaration of competing interest

The authors declare that they have no known competing financial interests or personal relationships that could have appeared to influence the work reported in this paper.

Data availability

The complete datasets and scripts employed to execute and post-process the calculations presented in this paper are available in the open access Zenodo repository 10.5281/zenodo.10608509.

Acknowledgements

Computational resources were provided by CLOUD@POLITO, a project of Academic Computing within the Department of Control and Computer Engineering at Politecnico di Torino.

This work has been carried out under the auspices of the Italian National Group of Mathematical Physics (Gruppo Nazionale di Fisica Matematica, GNFM) of the National Institute of High Mathematics (Instituto Nazionale di Alta Matematica, INDAM).

Appendix. Additional figures

See Figs. 26–32.

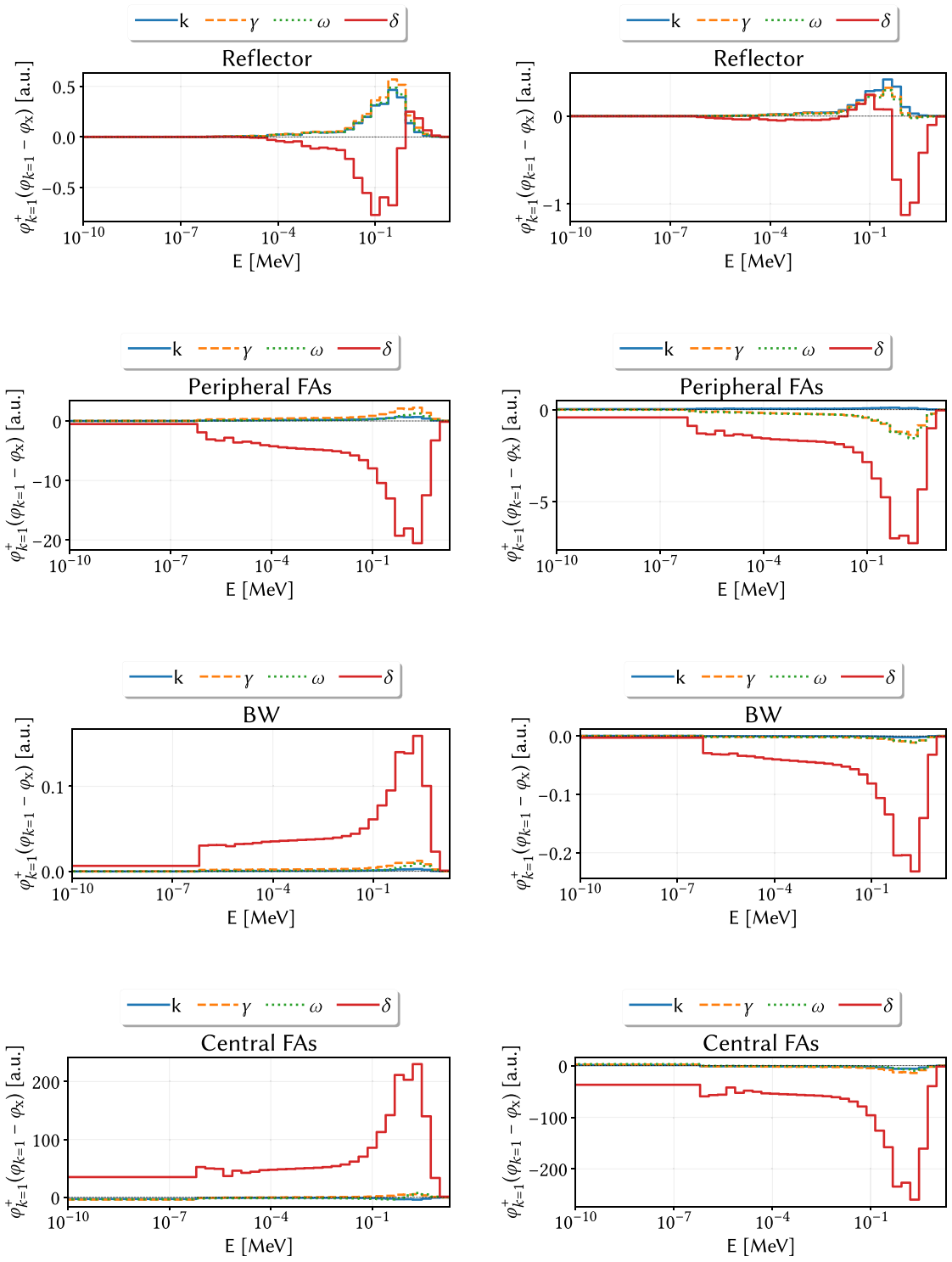


Fig. 26. Relative difference between the critical spectrum $\varphi_{k=1}$ (N_x = 140, P_3, Mark boundary conditions) and the spectra of the same system with higher (left, +2.5%) and lower (right, −2.5%) fission cross section for the LWR case.

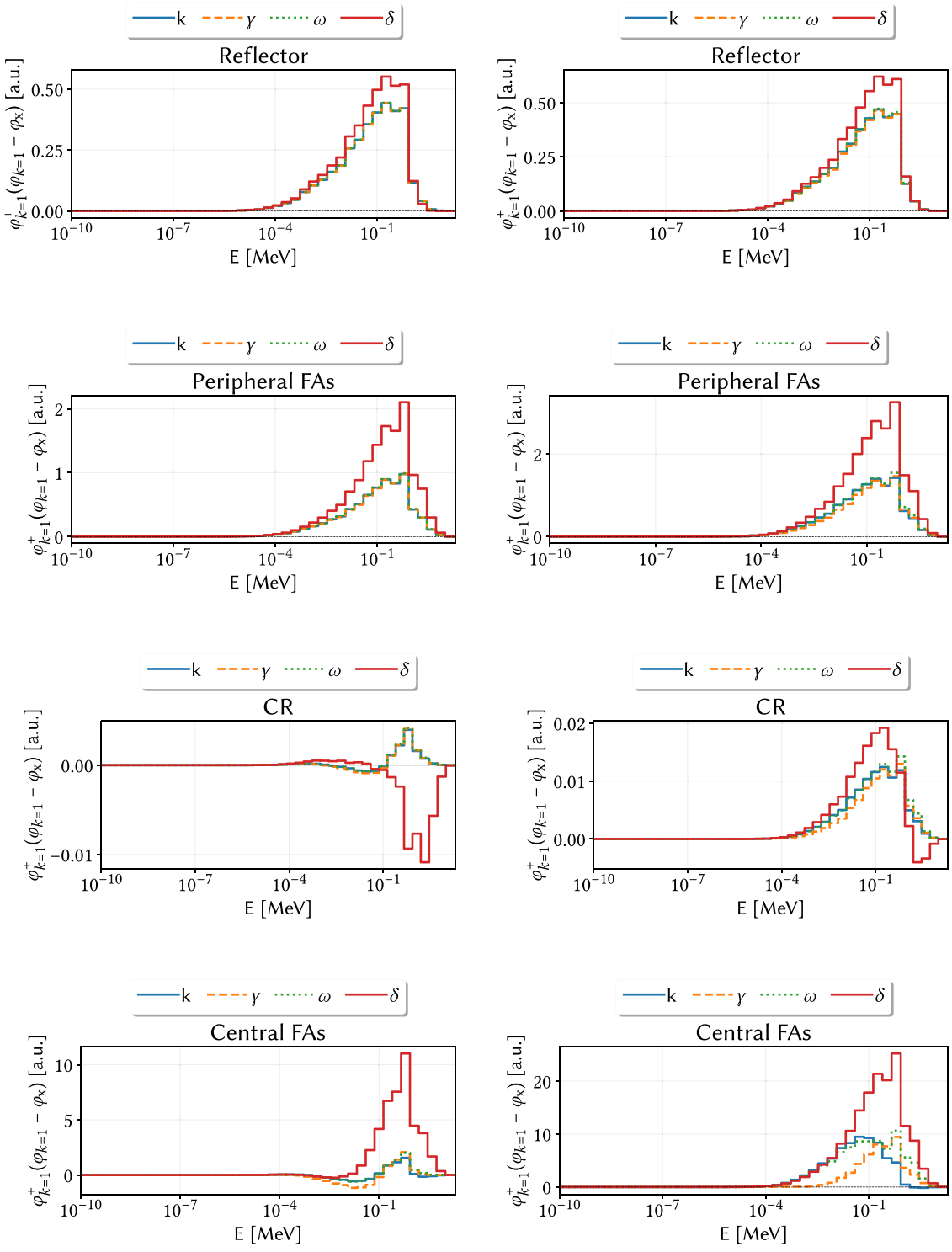


Fig. 27. Relative difference between the critical spectrum $\varphi_{k=1}$ (N_x = 140, P_3, Mark boundary conditions) and the spectra of the same system with higher (left, +2.5%) and lower (right, −2.5%) capture cross section for the LFR case.

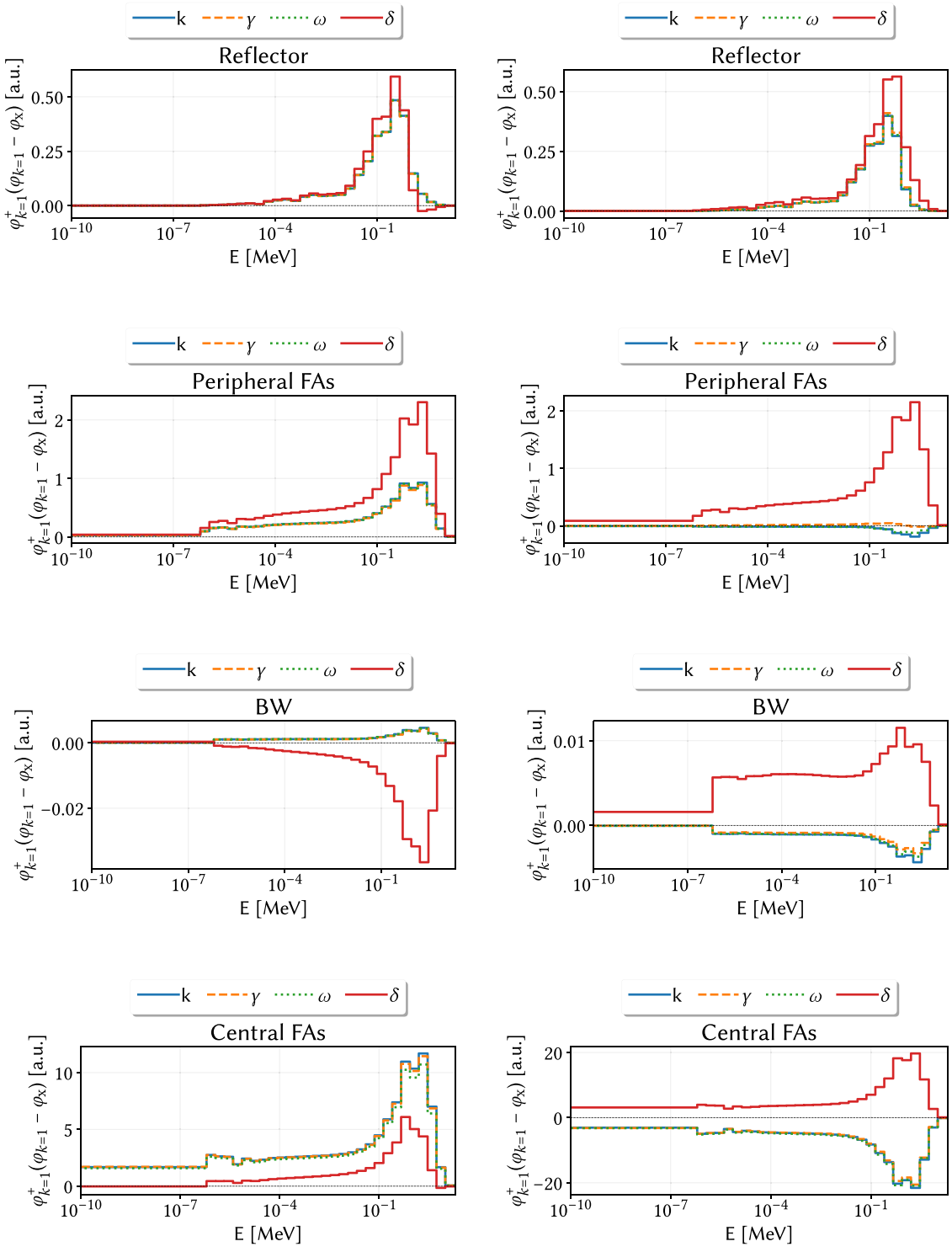


Fig. 28. Relative difference between the critical spectrum $\varphi_{k=1}$ (N_x = 140, P_3, Mark boundary conditions) and the spectra of the same system with higher (left, +2.5%) and lower (right, −2.5%) capture cross section for the LWR case.

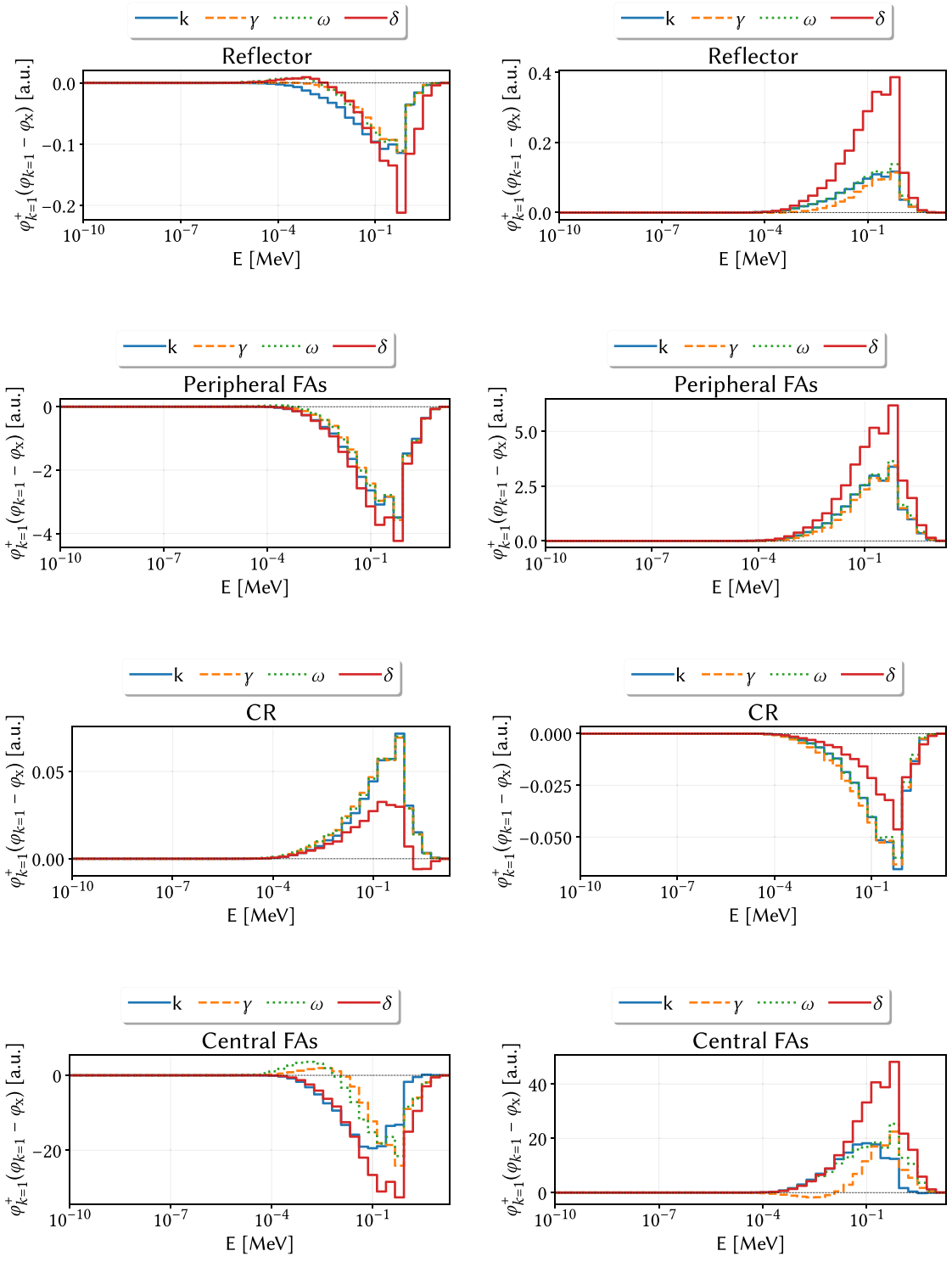


Fig. 29. Relative difference between the critical spectrum $\varphi_{k=1}$ ($N_x = 140$, P_3, Mark boundary conditions) and the spectra of the same system with thicker (left, +2.5%) and thinner (right, −2.5%) absorber layer for the LFR case.

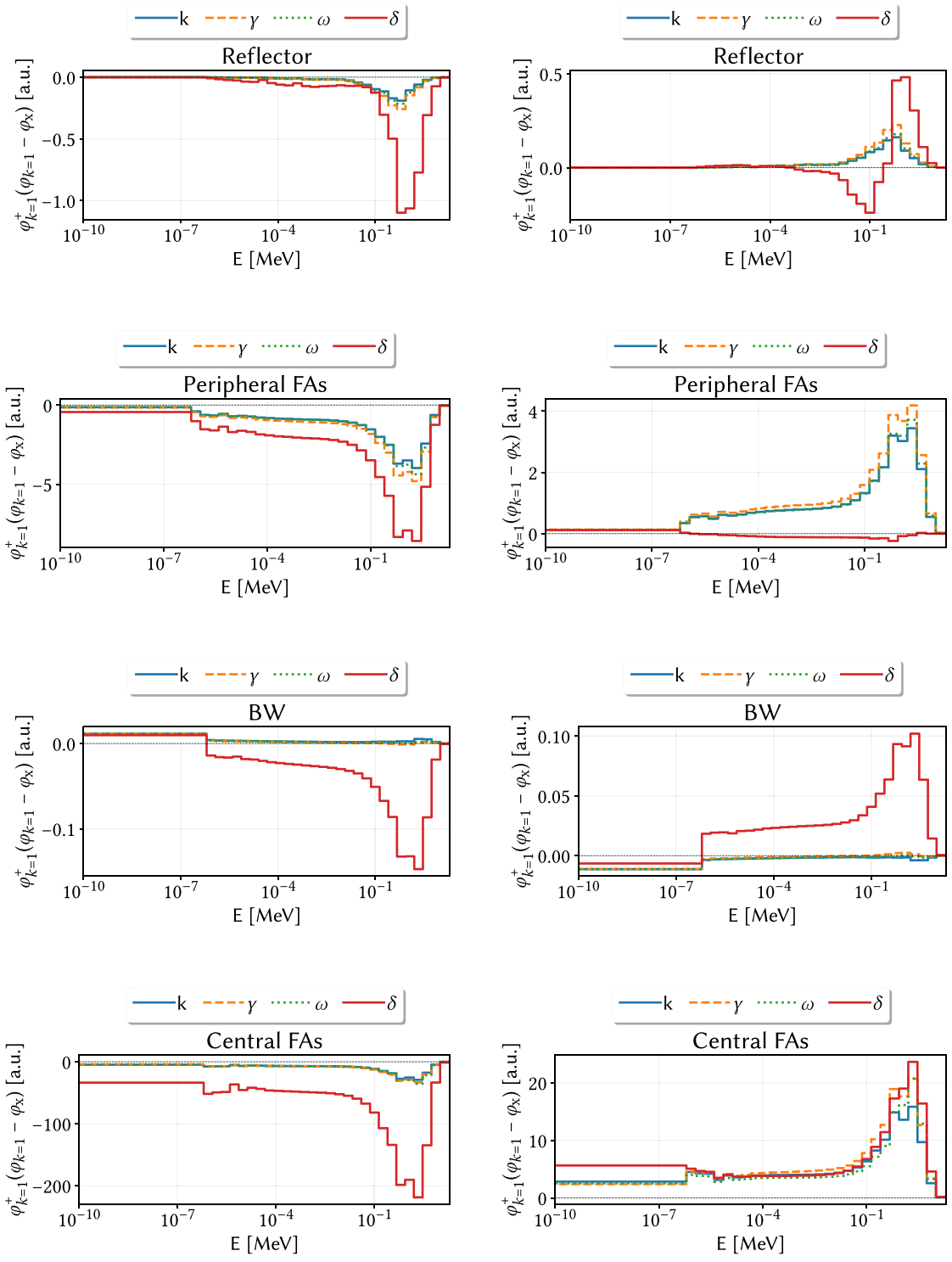


Fig. 30. Relative difference between the critical spectrum $\varphi_{k=1}$ ($N_x = 140$, P_3, Mark boundary conditions) and the spectra of the same system with thicker (left, +2.5%) and thinner (right, −2.5%) borated water layer for the LWR case.

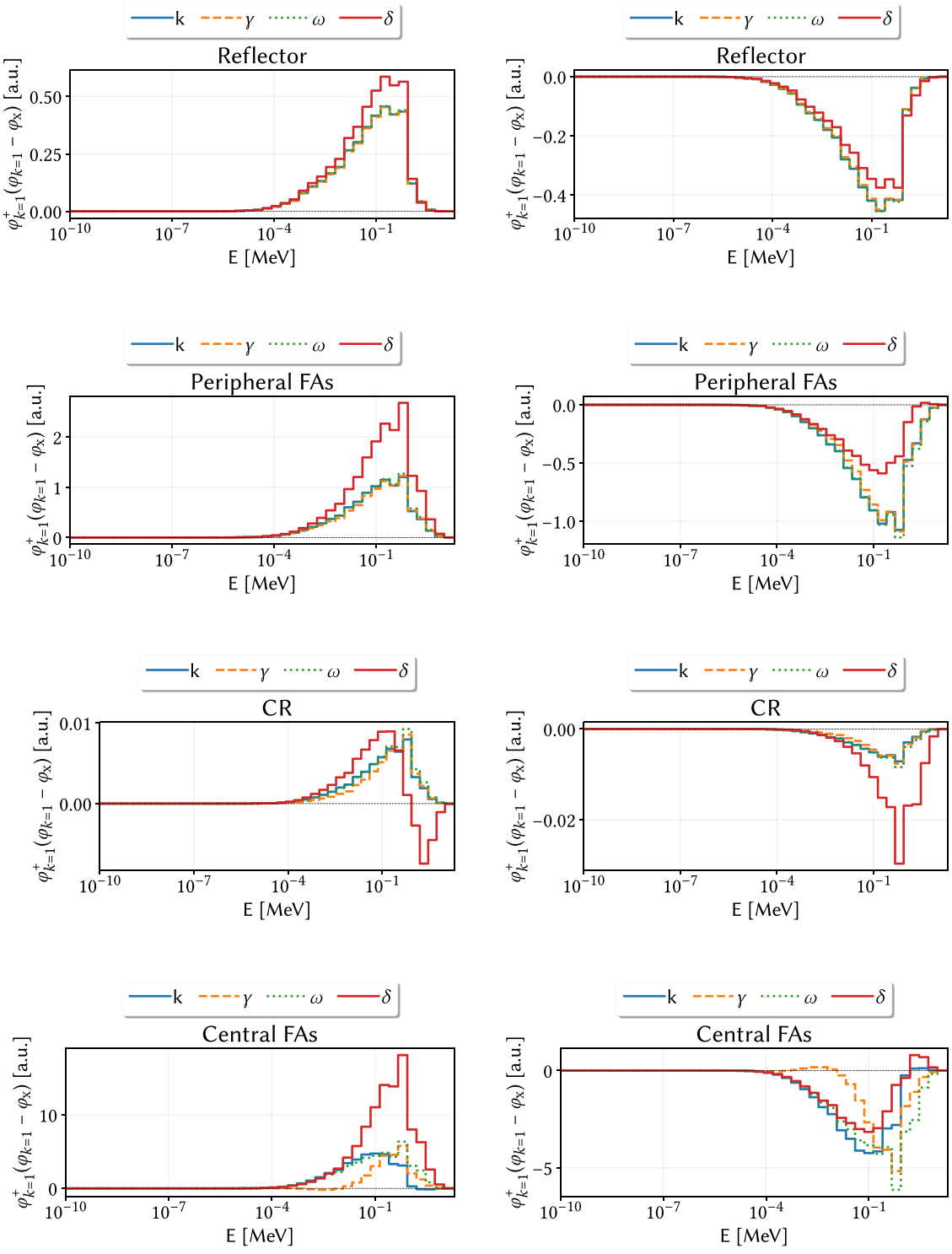


Fig. 31. Relative difference between the critical spectrum $\varphi_{k=1}$ (N_x = 140, P_3, Mark boundary conditions) and the spectra of the same system with thicker (left, +2.5%) and thinner (right, −2.5%) reflectors for the LFR case.

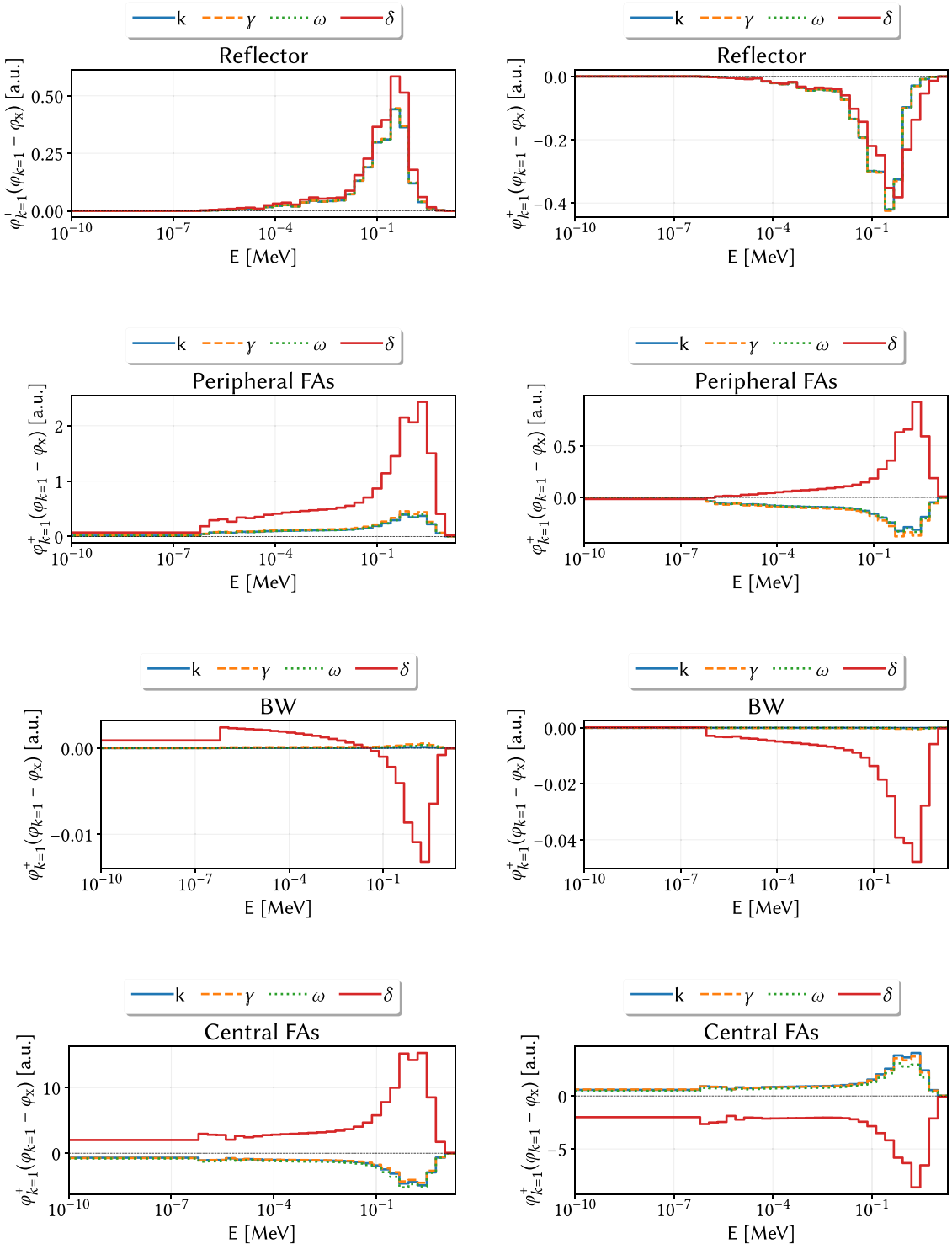


Fig. 32. Relative difference between the critical spectrum $\varphi_{k=1}$ ($N_x = 140$, P_3, Mark boundary conditions) and the spectra of the same system with thicker (left, +2.5%) and thinner (right, −2.5%) reflectors for the LWR case.

References

Abrate, N., Bruna, G., Dulla, S., Ravetto, P., 2019. Assessment of numerical methods for the evaluation of higher-order harmonics in diffusion theory. Ann. Nucl. Energy 128, 455–470, URL https://doi.org/10.1016/j.anucene.2019.01.011.

Abrate, N., Burrone, M., Dulla, S., Ravetto, P., Saracco, P., 2021a. Eigenvalue formulations for the P_N approximation to the neutron transport equation. J. Comput. Theor. Transp. 50, 407–429, URL https://doi.org/10.1080/23324309.2020.1856879.

Abrate, N., Dulla, S., Ravetto, P., Saracco, P., 2021b. On some features of the eigenvalue problem for the P_N approximation of the neutron transport equation. Ann. Nucl. Energy 163, 108–477, URL https://www.sciencedirect.com/science/article/pii/S0306454921003534.

Abrate, N., Dulla, S., Ravetto, P., Saracco, P., 2023. A generalized eigenvalue formulation for core-design applications. Nucl. Sci. Eng. 197, 1–25. http://dx.doi.org/10.1080/00295639.2022.2134685, arXiv:https://doi.org/10.1080/00295639.2022.2134685.

Bell, G.I., Glasstone, S., 1970. Nuclear Reactor Theory. Van Nostrand Reinhold, URL https://www.osti.gov/biblio/4074688.

Cacuci, D.G., Ronen, Y., Shayer, Z., Wagschal, J.J., Yeivin, Y., 1982. Eigenvalue-dependent neutron energy spectra: definitions, analyses, and applications. Nucl. Sci. Eng. 81, 432–442, URL https://doi.org/10.13182/NSE82-A20284.

Carreño, A., Vidal-Ferrándiz, A., Ginestar, D., Verdú, G., 2017. Spatial modes for the neutron diffusion equation and their computation. Ann. Nucl. Energy 110, 1010–1022, URL https://doi.org/10.1016/j.anucene.2017.08.018.

Carreño, A., Vidal-Ferràndiz, A., Ginestar, D., Verdú, G., 2019. Modal methods for the neutron diffusion equation using different spatial modes. Prog. Nucl. Energy (ISSN: 0149-1970) 115, 181–193. http://dx.doi.org/10.1016/j.pnucene.2019.03.040, URL https://www.sciencedirect.com/science/article/pii/S0149197019301052.

Case, K.M., 1960. Elementary solutions of the transport equation and their applications. Ann. Phys. 9 (1), 1–23, URL https://doi.org/10.1016/0003-4916(60)90060-9.

Chentre, N., Saracco, P., Dulla, S., Ravetto, P., 2018. Mathematical foundation of the neutron diffusion problem for a reflected nuclear reactor. Eur. Phys. J. Plus 133, 432.

Cullen, D.E., Little, R.C., Procassini, R., Clouse, C.J., 2003. Static and Dynamic Criticality: Are They Different? Technical Report UCRL-TR-201506 TRN: US0406611, Lawrence Livermore National Lab. (LLNL), Livermore, CA (U.S.A.), URL http://home.comcast.net/{~}redcullen1/Papers/Crits1/crits1.pdf.

Dahl, E.B., Protopopescu, V., Sjöstrand, N.G., 1983. On the relation between decay constants and critical parameters in monoenergetic neutron transport. Nucl. Sci. Eng. 83, 374–379, URL https://doi.org/10.13182/NSE83-A17570.

Davison, B., 1957. Neutron Transport Theory. Clarendon Press, Oxford, URL https://books.google.it/books/about/Neutron_Transport_Theory.html?id=ZhlRAAAAMAAJ&redir_esc=y.

Duderstadt, J.J., Hamilton, L.J., 1976. Nuclear Reactor Analysis. Wiley, New York, URL https://www.wiley.com/en-us/Nuclear+Reactor+Analysis-p-9780471223634.

Dugan, K., Sanchez, R., Zmijarevic, I., 2018. Cross section homogenization for transient calculations in a spatially heterogeneous geometry. Ann. Nucl. Energy (ISSN: 0306-4549) 116, 439–447. http://dx.doi.org/10.1016/j.anucene.2018.02.041, URL https://www.sciencedirect.com/science/article/pii/S0306454918300951.

Dugan, K., Zmijarevic, I., Sanchez, R., 2016. Cross-section homogenization for reactivity-induced transient calculations. J. Comput. Theor. Transp. (ISSN: 23324325) 45 (6), 425–441. http://dx.doi.org/10.1080/23324309.2016.1188116.

Dulla, S., Ravetto, P., Saracco, P., 2018. The time eigenvalue spectrum for nuclear reactors in multi-group diffusion theory. Eur. Phys. J. Plus 133, 1–24, URL https://doi.org/10.1016/j.pnucene.2012.03.002.

Fermi, E., 1942. Purpose of the Experiment at the Argonne Forest. Meaning of the Reproduction Factor "k". Technical Report CP-283 (Chicago Project Report), Chicago University, Metallurgical Laboratory, Chicago, IL, URL http://operedigitali.lincei.it/Fermi/Fermi-omnia2_testo.pdf.

Hanh, O., Strassmann, F., 1939. Über den nachweis und das verhalten der bei der bestrahlung des urans mittels neutronen entstehenden erdalkalimetalle. Naturwissenschaften 27, 11–15. http://dx.doi.org/10.1126/science.105.2715.27, URL https://link.springer.com/article/10.1007/BF01488241.

Henry, A.F., 1958. The application of reactor kinetics to the analysis of experiments. Nucl. Sci. Eng. 3, 52–70, URL https://doi.org/10.13182/NSE58-1.

Henry, A.F., 1964. The application of inhour modes to the description of non-separable reactor transients. Nucl. Sci. Eng. 20, 338–351, URL https://doi.org/10.13182/NSE64-A19579.

Kiedrowski, B.C., 2012. Evaluation of Computing c-Eigenvalues with Monte Carlo. In: ANS Annual Meeting, Chicago, IL (U.S.A.). American Nuclear Society, URL https://mcnp.lanl.gov/pdf_files/TechReport_2012_LANL_LA-UR-12-00577_Kiedrowski.pdf.

Kiedrowski, B.C., 2014. Comparison of prompt kinetics models derived from alternate eigenvalues. In: ANS Annual Meeting, Reno, NE (U.S.A.). American Nuclear Society, URL https://mcnp.lanl.gov/pdf_files/TechReport_2013_LANL_LA-UR-13-29496_Kiedrowski.pdf.

Leppänen, J., Pusa, M., Viitanen, T., Valtavirta, V., Kaltiaisenaho, T., 2015. The serpent Monte Carlo code: Status, development and applications in 2013. Ann. Nucl. Energy 82, 142–150. http://dx.doi.org/10.1016/j.anucene.2014.08.024.

Lewins, J., 1965. Importance: The Adjoint Function. The Physical Basis of Variational and Perturbation Theory in Transport and Diffusion Problems. Pergamon Press, Oxford.

Lewis, E.E., Miller, W.F., 1984. Computational Methods of Neutron Transport. Wiley, New York, URL https://www.osti.gov/biblio/5538794.

McClarren, R.G., 2019. Calculating time eigenvalues of the neutron transport equation with dynamic mode decomposition. Nucl. Sci. Eng. 193 (8), 854–867, URL https://doi.org/10.1080/00295639.2018.1565014.

Perel, R.L., Wagschal, J.J., Yeivin, Y., 1999. One group transport calculations revisited. In: Conference of the Nuclear Societies in Israel, Dead Sea, Israel. pp. 33–36, URL https://inis.iaea.org/collection/NCLCollectionStore/_Public/31/049/31049517.pdf?r=1.

Pomraning, G.C., 1989. The transport equation in general geometry. Nucl. Sci. Eng. 101 (4), 330–340.

Ravetto, P., 1974. Metodi Analitici Per la Dinamica Spaziale di Sistemi Non Omogenei (Master's thesis). Politecnico di Torino.

Ronen, Y., Shalitin, D., Wagschal, J.J., 1976. A useful different eigenvalue for the transport equation. Trans. Am. Nucl. Soc. (24), 474, URL https://inis.iaea.org/search/search.aspx?orig_q=RN:8305018.

Sahni, D.C., Sjöstrand, N.G., 1990. Criticality and time eigenvalues in one-speed neutron transport. Prog. Nucl. Energy 23, 241–289, URL https://doi.org/10.1016/0149-1970(90)90004-O.

Sahni, D.C., Sjöstrand, N.G., Garis, N.S., 1995. Spectrum of one-speed neutron transport operator with reflective boundary conditions in slab geometry. Transport Theory Statist. Phys. 24, 629–656, URL https://doi.org/10.1080/00411459508206019.

Sanchez, R., Tomatis, D., 2019. Analysis of α modes in multigroup transport. In: International Conference on Mathematics and Computational Methods Applied to Nuclear Science and Engineering, M&C 2019, Portland, OR (U.S.A.). pp. 1134–1143.

Sanchez, R., Tomatis, D., Zmijarevic, I., Joo, H.G., 2017. Analysis of alpha modes in multigroup diffusion. Nucl. Eng. Technol. 49, 1259–1268, URL https://doi.org/10.1016/j.net.2017.07.007.

Saracco, P., Dulla, S., Ravetto, P., 2012. On the spectrum of the multigroup diffusion equations. Prog. Nucl. Energy 59, 86–95, URL https://doi.org/10.1016/j.pnucene.2012.03.002.

Singh, K.P., Degweker, S.B., Modak, R.S., Singh, K., 2011. Iterative method for obtaining the prompt and delayed alpha-modes of the diffusion equation. Ann. Nucl. Energy 38, 1996–2004, URL http://dx.doi.org/10.1016/j.anucene.2011.04.018.

Velarde, G., Ahnert, C., Aragonés, J.M., 1978. Analysis of the eigenvalue equations in k, λ, γ, and α applied to some fast- and thermal-neutron systems. Nucl. Sci. Eng. 66, 284–294, URL https://doi.org/10.13182/NSE78-A27213.

Vitali, V., 2020. Monte Carlo Analysis of Heterogeneity and Core Decoupling Effects on Reactor Kinetics: Application to the EOLE Critical Facility (Ph.D. thesis). Université Paris-Saclay, URL http://www.theses.fr/2020UPASP045.

Weinberg, A.M., Wigner, E.P., 1958. The Physical Theory of Neutron Chain Reactors. University of Chicago Press, Chicago, URL https://books.google.it/books/about/The_Physical_Theory_of_Neutron_Chain_Rea.html?id=IwwjAAAAMAAJ&redir_esc=y.

Zoia, A., Brun, E., Malvagi, F., 2014. Alpha eigenvalue calculations with TRIPOLI-4. Ann. Nucl. Energy 63, 276–284, URL https://doi.org/10.1016/j.anucene.2013.07.018.